NASA TECHNICAL NOTE

NASA TN D-8040

NASA TN D-8040

THEORETICAL FACE PRESSURE AND DRAG CHARACTERISTICS OF FORWARD-FACING STEPS IN SUPERSONIC TURBULENT BOUNDARY LAYERS

D. K. Patel and K. R. Czarnecki

Langley Research Center
Hampton, Va. 23665

NATIONAL AERONAUTICS AND SPACE ADMINISTRATION • WASHINGTON, D. C. • DECEMBER 1975

THEORETICAL FACE PRESSURE AND DRAG CHARACTERISTICS OF FORWARD-FACING STEPS IN SUPERSONIC TURBULENT BOUNDARY LAYERS

D. K. Patel* and K. R. Czarnecki
Langley Research Center

SUMMARY

A theoretical investigation has been made of the pressure distributions on and drag characteristics of the faces of forward-facing steps immersed in turbulent boundary layers at supersonic speeds. An approximate solution technique proposed by Uebelhack has been modified and extended to obtain a more consistent numerical procedure.

Numerical results obtained indicate that decreases in the assumed separation angle and increases in the assumed shear-layer spreading parameter result in decreased pressure levels and drag forces. Increases in the index of the assumed power-law velocity profiles caused small increases in the dividing streamline pressures at the smaller ratios of step height to boundary-layer thickness but had no significant effect on the drag. Modifications to the width of the shear layer and reverse-flow pressure distributions resulted in reasonably good agreement between theoretical and experimental face pressure distributions for moderate ratios of step height to boundary-layer thickness (from 2 to 7). By coupling a decrease in assumed separation angle with an increase in the shear-layer spreading parameter, the modified theory can be extended empirically to give good agreement between theory and experiment for ratios of step height to boundary-layer thickness as low as 0.05 at free-stream Mach numbers of 1.61 and 2.20. There is some disagreement between the results obtained in this investigation and those of Uebelhack which apparently cannot be ascribed to different methods of computation.

INTRODUCTION

The study of supersonic turbulent boundary-layer separation due to a forward-facing step has many useful applications. At low ratios of step height to boundary-layer thickness, the data and analytical procedures are helpful in assessing the effects of manufacturing discontinuities on aircraft drag and performance, at larger ratios, the results can be used to predict the effectiveness of spoilers and deceleration devices. The separation phenomena have been extensively investigated both theoretically and experimentally, yet in neither case

---

*NRC-NASA Resident Research Associate.

has much emphasis been focused on the flow at or near the step face From the standpoint of theory this lack of emphasis stems primarily from the complexity of the problem. The lack of experimental attention results from the very small models that usually must be used which makes it very difficult to install a sufficient number of static orifices to reasonably determine the pressure distribution over the step face. Inasmuch as the flow near the step face determines the drag characteristics of forward-facing steps, a need exists to investigate this flow region. A logical first step appeared to be a study of the utility of the theory proposed by Uebelhack (ref. 1), the results of this study are the subject of the present paper.

Uebelhack's theory is based on a highly simplified phenomenological model but appears to be in good agreement with experimental results. The theory is stated to be applicable only for ratios of step height to boundary-layer total thickness of greater than 2 (ref. 1) Also the theory provides an average pressure for the step face and a peak or reattachment pressure which is the stagnation pressure on the streamline dividing the flow passing over the step from that being recirculated in the separated-flow region In this study the implications of the theory as to the pressure distributions on the step face are examined and the requirements for extending the usefulness of the theory to lower ratios of step height to boundary-layer thickness are established. In addition, variations in the basic parameters are investigated in more detail than by Uebelhack and some errors in procedure and experimental data interpretation are corrected. Calculations were made over a Mach number range from 1.61 to 6.0, over a range of ratios of step height to boundary-layer total thickness from 0.001 to ∞, and over a range of boundary-layer velocity profiles from the 1/7 to the 1/11 power laws.

SYMBOLS

a_0, a_1, a_2, a_3 arbitrary constants (eq. (13))

C_a Crocco number, $\frac{u_a}{u_{max}} = \frac{u_{2,e}}{u_{max}}$

C_D drag coefficient

d dividing streamline

h step height

j inviscid jet boundary streamline

M Mach number

m	mass, center of mixing
N_{Pr}	Prandtl number
n	power-law exponent for velocity profile
p	pressure
$R_{\delta 1}$	Reynolds number
T_o	total temperature
u	velocity along x-axis
v	velocity along y-axis
x	longitudinal coordinate in original coordinate system (fig. 20)
x_o	correction for mixing length (eq. (A25))
x*	length of the mixing region (fig 1)
$\bar{x}$	longitudinal coordinate in modified coordinate system or effective length of mixing region (fig 20)
y	lateral or step coordinate
β	shock-wave angle, degrees
γ	specific-heat ratio
δ	boundary-layer thickness
δ^*	boundary-layer displacement thickness
η	dimensionless coordinate, $y\sigma/x$
$\bar{\eta}$	dimensionless coordinate, $y\sigma/\bar{x}$

θ boundary-layer momentum thickness

θ_s separation angle, degrees

ρ density

σ shear-spreading parameter (eq. (2))

ϕ velocity ratio, $\frac{u_2}{u_a} = \frac{u_2}{u_{2,e}}$

Subscripts:

a region of higher velocity in two mixing streams (identical to region above the shear layer behind the oblique separation shock)

b region of lower velocity in two mixing streams, also region of reverse flow

d dividing streamline

e boundary-layer edge

j inviscid jet boundary streamline values

m center of mixing

max maximum

o stagnation conditions

ra,rb large positive and negative reference (fig. 18)

1 ahead of oblique separation shock (free stream)

2 behind oblique separation shock

THEORETICAL APPROACH

The calculation of the pressures on the front of a forward-facing step is based on Uebelhack's shear-flow model which is shown schematically in figure 1. As the flow approaches the step face, the boundary-layer flow separates from the plane wall, inducing an oblique shock. Behind the shock, the boundary layer is assumed to change to a free shear flow inclined at a constant separation angle θ_s to the surface. The shear flow expands as it proceeds downstream and reattaches to the step face with part of the flow passing over the step and part of the flow being reversed in direction in the separated-flow region near the wall. No physical mechanism is provided for reversing the flow. For analysis, the basic flow model is divided into the following four regions

(1) Separation region

(2) Free-mixing region

(3) Reattachment region

(4) Reverse-flow region

The concepts and most important assumptions used to analyze the individual regions are described briefly in this section. (For a more detailed description of the method, see ref. 1.) A concise derivation of the basic equations is presented in appendix A and a description of the calculation procedure is presented in appendix B. Uebelhack's derivation of the basic equations is repeated in this section since some modifications were made to the procedure as well as corrections of a number of typographical errors in reference 1.

(1) Separation Region

The flow separates from the wall before reaching the step face at a distance determined by the separation angle θ_s (fig. 1). This angle is determined from correlation of experimental results (ref. 1). At the separation point an oblique shock is induced. Ahead of the shock, the boundary layer is characterized in terms of δ_1, δ_1^*, and θ_1. Behind the shock, the new boundary-layer characteristics are calculated by use of the oblique-shock theory. The boundary-layer momentum thickness behind the shock θ_2 is the important parameter connecting mass and momentum flux. In terms of the initial boundary-layer characteristics and flow-separation parameter θ_2 is found to be

$$\theta_2 = -\frac{1}{\cos\theta_s}\left[\left(\delta_1 - \delta_1^* - \theta_1\right)\frac{\sin\left(\beta - \theta_s\right)}{\sin\beta}\,\frac{\cos\left(\beta - \theta_s\right)}{\cos\beta}\right.$$

$$\left. - \left(\delta_1 - \delta_1^*\right)\frac{\sin\left(\beta - \theta_s\right)}{\sin\beta}\cos\theta_s + \delta_1\,\frac{p_1 - p_2}{\gamma p_2 M_{2,e}^2}\right] \tag{1}$$

where β is the oblique shock angle (fig. 1), p_1 and p_2 are the static pressures ahead of and behind the shock, respectively, and $M_{2,e}$ is the Mach number outside the boundary layer behind the shock

(2) Free-Mixing Region

The boundary layer behind the oblique shock is assumed to change instantaneously to a shear layer having the same momentum thickness as the boundary layer immediately behind the shock. For simplicity, the following assumptions are made.

(1) The shear layer expands linearly.

(2) The mixing occurs at the constant static pressure p_2.

(3) The shear-layer velocity distribution can be approximated by an error-function profile.

(4) The flow is isoenergetic with unit Prandtl number $\left(T_o = \text{Constant},\ N_{Pr} = 1\right)$.

The linearly spreading shear layer requires the use of a spreading or mixing parameter σ which is based on experimental correlations. For this investigation σ was taken according to Korst and Chow's suggestion for compressible fluids (ref. 2):

$$\sigma = 12 + 2.76M_{2,e} \tag{2}$$

Reference 3 presents a more recent correlation which yields values of σ nearly twice as large as those indicated by equation (2). The recommended correlation is, however, highly tentative and intended for fully developed shear layers, whereas for practical ratios of step height to boundary-layer thickness ($h/\delta < 5$), the experimental shear layer generally cannot be expected to be fully developed. Equation (2) yields results that appear to be in reasonable agreement with the still developing shear layers of reference 3. For $h/\delta_1 \geq 5$, the shear layer may become more fully developed and higher σ values may be appropriate.

The shear layer must be properly located· specification that the momentum thickness of the shear layer be equal to that of the boundary layer places the shear layer at the correct longitudinal location; specification of the angle θ_s aligns the layer at the desired angle with reference to the wall. Proper location of the center of the shear layer normal to the wall at the separation point requires two adjustments. The first of these is concerned with the fact that as the shear layer grows in width in the downstream direction from the virtual origin, the center of the layer, which is specified in terms of the symmetry of the velocity profile, is continuously displaced in a normal direction away from the initial position at the virtual origin. The adjustment is calculated by invoking the laws of conservation of mass and momentum within a control volume enclosing the upper and lower bounds of the shear layer. (See appendix A.) The second adjustment must account for the thickness of the boundary layer immediately behind the separation shock. This adjustment is accomplished by the assumed injection of air into the region below the shear layer to account for the momentum thickness of the boundary layer (See appendix A.)

(3) Reattachment Region

As the shear flow approaches the step, a part of the flow reattaches to the step face, while the remainder passes over the step (fig. 1) The streamline that identifies these two parts of the flow is defined as the dividing or reattachment streamline and the assumption is made that this streamline reattaches at the outer corner of the step. The present theory does not provide any physical mechanism for reversing the flow. In effect, the assumption is made that the flow in the reattaching shear layer below the dividing streamline can be stagnated without any turning of the flow or spreading of the streamlines. This procedure allows the retarding force on the step face to be calculated at the price of the unaccounted-for disappearance of the mass flow contained in this part of the shear layer.

(4) Reverse-Flow Region

In the Uebelhack separated-flow model, the flow beneath the shear layer is assumed to be reversed at constant velocity (fig. 1) with constant static pressure p_2 behind the separation shock. The mass flow in this region is equated to the mass flow in the reattaching shear layer below the dividing streamline at the step face. This procedure allows evaluation of the force on the step face adjacent to this region required to accelerate the subject mass flow from zero velocity to the final reverse-flow velocity; again the mass flow must appear unaccountably at the step face.

Inasmuch as the experimental data do not indicate uniform reverse-flow velocities, the theory was modified for some calculations with the assumption that the pressure distributions in the reverse-flow region are mirror images of those in the shear-layer portion of the step

face with the focal or turning point located at half the step height This approach will be defined as the "variable η_{rb}" method.

Final Equations

One of the final results of the analysis is an integral over the pressure distribution on the step face. This integral is

$$\int_0^1 \frac{p - p_2}{p_2}\,\frac{dy}{h} = \gamma M_{2,e}^2\,\frac{\bar{x}}{\sigma h}\left\{\int_{\bar{\eta}_{rb}}^{\bar{\eta}_d} \frac{\left(1 - C_a^2\right)\phi^2}{1 - C_a^2\phi^2}\,d\bar{\eta}\,\cos\theta_s + \frac{1}{1 - C_a^2}\left[\int_{\bar{\eta}_{rb}}^{\bar{\eta}_d} \frac{\left(1 - C_a^2\right)\phi}{1 - C_a^2\phi^2}\,d\bar{\eta}\right]^2 \frac{1}{\frac{\sigma h}{\bar{x}} - \left(\bar{\eta}_d - \bar{\eta}_{rb}\right)\cos\theta_s}\right\} \tag{3}$$

where

$\bar{x}$ longitudinal length of shear layer

$\bar{\eta}_d$ dimensionless coordinate for dividing streamline

$\bar{\eta}_{rb}$ arbitrary dimensionless coordinate at which the error-function velocity is very small

C_a $= u_{2,e}/u_{max}$, isoenergetic Crocco number

ϕ $= u_2/u_{2,e}$, error-function velocity ratio

$\bar{\eta}$ $= y\sigma/\bar{x}$, dimensionless lateral coordinate

h height of the step face

This pressure integral can be related to the free-stream static pressure existing ahead of the separation shock by

$$\int_0^1 \frac{p}{p_1}\,\frac{dy}{h} = \left(\int_0^1 \frac{p - p_2}{p_2}\,\frac{dy}{h} + 1\right)\frac{p_2}{p_1} \tag{4}$$

From the preceding pressure integral, the drag coefficient on the step face is calculated by

$$C_D = \frac{\int_0^1 \frac{p}{p_1}\,\frac{dy}{h} - 1}{\frac{1}{2}\gamma M_{1,e}^2} \tag{5}$$

Uebelhack (ref. 1) did not consider the effective pressure distribution on the step face except for the stagnation pressure on the dividing streamline. To calculate this pressure he used the equation

$$\frac{p_{o,d}}{p_1} = \left(1 + \frac{\gamma - 1}{2} M_d^2\right)^{\frac{\gamma}{\gamma-1}} \frac{p_2}{p_1} \tag{6}$$

where $p_{o,d}$ is the stagnation pressure at the end of the dividing streamline and M_d is the Mach number on the dividing streamline. The use of this equation, which applies to subsonic isentropic flows, is not compatible with the assumption of constant pressure and total temperature in the shear layer. Uebelhack does not specify his exact procedure for the case where the Mach number on the dividing streamline is supersonic. Because the implied pressure distributions on the step face were of interest in this investigation the correct equations for the pressures were derived from the pressure integral (eq. (3)) and are

$$\frac{p - p_2}{p_2} = \gamma M_{2,e}^2 \left[\frac{\left(1 - C_a^2\right)\phi^2}{1 - C_a^2\phi^2} \cos\theta_s\right] \tag{7}$$

for the shear-layer portion of the flow and

$$\frac{p - p_2}{p_2} = \gamma M_{2,e}^2 \left\{\frac{1}{1 - C_a^2}\left[\int_{\bar{\eta}_{rb}}^{\bar{\eta}_d} \frac{\left(1 - C_a^2\right)\phi}{\left(1 - C_a^2\phi^2\right)}\, d\eta \, \frac{1}{\frac{\sigma h}{\bar{x}} - \left(\bar{\eta}_d - \bar{\eta}_{rb}\right)\cos\theta_s}\right]^2\right\} \tag{8}$$

for the reverse-flow portion of the step. Equation (4) is modified in equations (7) and (8) to the form

$$\frac{p}{p_1} = \left(\frac{p - p_2}{p_2} + 1\right)\frac{p_2}{p_1} \tag{9}$$

When the free-stream Mach number and step height are sufficiently large, a part of the shear layer in the separated-flow region is supersonic (for example, for $h/\delta_1 > 2$ at $M_{1,e} = 5$). For all reattachment pressures in this case, but only for a few drag and pressure distribution calculations, it was assumed that this flow was decelerated through a normal shock. The equations given in reference 3 were utilized to obtain the pressure ratio $p_{o,d}/p_1$ when accounting for the normal shock. In the reverse-flow region, shocks cannot exist because the flow is accelerating.

RESULTS AND DISCUSSION

Constant η_{rb}

Comparison with Uebelhack's results.- A comparison of the results computed in this investigation with those of Uebelhack is presented in figure 2. Here, the dividing-streamline stagnation or reattachment pressure $p_{o,d}/p_1$ and drag coefficient C_D are plotted as a function of free-stream Mach number $M_{1,e}$ and the ratio of step height to free-stream total boundary-layer thickness (step-height ratio) h/δ_1. For a direct comparison with Uebelhack's results, the same basic approach with constant η_{rb} was utilized and the dividing-streamline pressure ratio was computed by the same isentropic flow procedure used by Uebelhack in his calculations. If the dividing-streamline Mach number is higher than 1, a normal shock is taken into account for the $p_{o,d}/p_1$ calculation. The calculations were made for a range of $M_{1,e}$ from 2 to 6 and for a range of h/δ_1 from 0.1 to 100 (essentially ∞).

The curves show that the present results are in only fair agreement with Uebelhack's results. The $p_{o,d}/p_1$ curves of the present investigation are more linear and more uniformly spaced in both the Mach number and h/δ_1 plots. In the case of C_D, Uebelhack's results show more variation with h/δ_1 than the present calculations and, in fact, show an increase in C_D with a decrease in h/δ_1 which is contrary to expectation. The reasons for the major part of these discrepancies, which are unexpected because the same basic equations are used for the calculations, are not known.

Note that the curves indicate that C_D and $p_{o,d}/p_1$ asymptotically approach limiting values as $h/\delta_1 \to \infty$. The reason for this is that for very large step-height ratios, the boundary-layer thickness is only a minute part of the step height. The boundary layer provides for the separation of the flow but the detail characteristics of the initial boundary layer fade into insignificance. Thus, Reynolds number effects may be expected to exist for low values of h/δ_1 but little or no effects are to be expected for higher values of h/δ_1.

The static pressures and the drag coefficients corresponding to these static pressures which result from turning the free-stream flow through the separation angle θ_s are also shown in figure 2. This makes it possible to determine the relative contribution of the static and dynamic pressures to the drag coefficient and dividing-streamline stagnation pressure.

The results indicate that the contribution of the dynamic pressure is low for low Mach numbers and low values of h/δ_1, and high for high Mach numbers and high values of h/δ_1.

Effects of changes in θ_s and σ.- In order to apply the theory, two empirical factors, the separation angle θ_s and the spreading factor σ, are used. These are based on correlations of questionable accuracy; consequently, figures 3 and 4 have been prepared to indicate the sensitivity of the present method to changes in these two parameters. Calculations are presented in figure 3 for $\theta_s + 1°$ and $\theta_s - 1°$ and in figure 4 for 0.9σ and 1.1σ, where the values of θ_s and σ are adopted from reference 1.

A decrease of 2° in θ_s (fig. 3) results in a significant decrease in the dividing-streamline stagnation pressure and in the drag coefficient. The effect is largest for the highest step-height ratios and free-stream Mach numbers

An increase of approximately 20 percent in the value of σ (fig. 4) decreases appreciably the values of the dividing-streamline stagnation pressure and drag coefficient. The strongest effect occurs at the lowest step-height ratios and highest free-stream Mach numbers. A study of more recent correlations for σ (ref. 3) indicates that σ probably should be a function of h/δ_1, $R_{\delta 1}$, and Mach number and this could have some influence on the shape of the drag curves for $h/\delta_1 > 5$.

Effects of changes in velocity profile.- The effects of the changes in the power of the velocity profile from 1/7 to 1/9 to 1/11 are illustrated in figure 5. As expected there is only a small effect of the change of the velocity profile at the higher values of h/δ_1, but the effect becomes stronger as h/δ_1 decreases For $p_{o,d}/p_1$, the greatest change, an increase with increase in power index, occurs at the highest Mach number, for C_D, the largest change, a decrease with increase in power index, occurs at the lowest Mach number The maximum variation in $p_{o,d}/p_1$ and C_D is less than 8 percent

Pressure distributions.- The pressure integral used to calculate the step-drag coefficient implies a certain pressure distribution on the step face. This pressure distribution is made up of two components, the static pressure due to turning the stream flow through the separation angle θ_s and the pressure derived by stagnating the flow in the shear layer as well as reverse-flow region. Some typical implied pressure distributions are shown in figure 6 for a range of ratios of step height to boundary-layer thickness for Mach numbers of 3 and 6. For reasons that will be discussed later, the assumption was made that there were no normal shocks in the flow even if the flow was somewhere supersonic. For a particular step-height ratio the pressure distribution region is divided into two parts. One is in the shear-layer region and another is in the reverse-flow region. In the shear-layer region, the step-face pressure decreases from the dividing-streamline stagnation or peak pressure nearly exponentially toward the static pressure of separation. In the reverse-flow region, the step-face pressure is uniform everywhere because of the assumption of uniform velocity and uniform static

pressure behind the separation shock. There is a discontinuity in the flow at the junction of the shear layer and reverse-flow region. The results also indicate that the step-face pressures are of higher magnitude for higher Mach numbers with the dynamic pressure component increasing in importance.

As h/δ_1 decreases, the dividing-streamline stagnation pressure decreases, but the shear-layer height on the step face increases. Thus the reverse-flow height on the step face also decreases and results in higher dynamic pressures in this region. For very small values of h/δ_1, the pressures in the reverse-flow portion exceed the peak pressure at the outer corner. (See fig. 6.) This is physically impossible and explains the rapid rise of the curve of drag coefficient with decreasing h/δ_1. (See fig. 2(b).) Use of energy conservation would probably yield an improved estimate of the pressure in the reverse-flow region but with an increase in complexity.

Variable η_{rb}

Pressure distribution.- The previous problem is bypassed by fixing the junction of the shear layer and the reverse-flow region at the center of the step face. For this condition, the η_{rb} is not kept constant, but is allowed to vary so as to satisfy the previous condition. The resulting pressure distributions calculated by this method are shown in figure 7 for Mach numbers of 3 and 6 for the same range of h/δ_1 as in figure 6. In the shear-layer region, the pressure distributions are almost the same as those in figure 6, but in the reverse-flow region, the pressure distributions are essentially independent of h/δ_1. This characteristic tends strongly to delay the breakdown of the numerical calculations for low step-height ratios, but the theory must still ultimately deteriorate as h/δ_1 decreases because the pressure integral (eq. (3)) is singular for $h/\delta_1 = 0$.

Reattachment pressures and drag coefficients.- Figures 8(a) and 8(b) show comparisons of the dividing-streamline pressures and drag coefficients calculated by both the variable and constant η_{rb} methods. For both methods, the pressure ratio $p_{o,d}/p_1$ was computed by means of the isentropic equation (6). For the case of $p_{o,d}/p_1$, there is no significant difference between the results of the two methods for $h/\delta_1 > 1.0$. However, for $h/\delta_1 < 1.0$, the variable η_{rb} method generates $p_{o,d}/p_1$ values that are higher than those calculated by the constant η_{rb} method. The variable η_{rb} method results in somewhat higher C_D values at the higher values of h/δ_1 and lower values at lower h/δ_1 values, cumulating in a curve that shows a decreasing drag with decreasing h/δ_1 and is more in agreement with experimental trends Also, the tendency of the theory to break down (as evidenced by the upturning of the drag curves at the lower values of h/δ_1) is delayed to at least an order of magnitude decrease in step-height ratio and suggests the possibility of extending the usefulness of the theory to these lower values of h/δ_1.

Reattachment pressure derived from pressure integral.- The use of Crocco's integral or relationship between velocities and densities with the static pressure and stagnation temperature held constant yields the relationship

$$\frac{\rho_2}{\rho_a} = \frac{1 - C_a^2}{1 - C_a^2\phi^2} \tag{10}$$

The use of the isentropic relationship in equation (6) (for shockless flow)

$$\frac{p_{o,d}}{p_1} = \left(1 + \frac{\gamma - 1}{2}M_d^2\right)^{\frac{\gamma}{\gamma-1}} \frac{p_2}{p_1}$$

cannot satisfy both these requirements simultaneously. For a constant-stagnation-temperature adiabatic process, the density relationship can be shown to be (ref. 4)

$$\frac{\rho_2}{\rho_a} = \left(\frac{1 - C_a^2}{1 - C_a^2\phi^2}\right)^{\frac{1}{\gamma-1}} \tag{11}$$

In equations (10) and (11), ρ_2/ρ_a increases as ϕ increases as required in the shear layer, but the rates of increase are completely different due to the different power index. Thus, $p_{o,d}/p_1$ calculated by equation (6) is not compatible with the problem. For this reason the reattachment pressures were also calculated directly from equation (7) $\left(\text{with } \phi = \phi_d\right)$ which was derived from Uebelhack's pressure integral. The results are presented in figure 9 and are compared with present calculations made by Uebelhack's method (eq. (6)).

The dividing-streamline stagnation pressure calculated by Uebelhack's method is not in agreement with that calculated by the integral equation. There is considerable difference in values at low Mach numbers and low values of h/δ_1. The integral method gives pressure ratios $p_{o,d}/p_1$ that are higher than those calculated by the Uebelhack's method for the lower Mach numbers and the ratios increase more slowly with the increase in Mach number. With the exception of $M_{1,e} = 6$, the integral method gives higher values of pressure than Uebelhack's method for the range of h/δ_1 considered.

Mach number on dividing streamline.- The Mach number on the dividing streamline is of interest since it indicates the type of equations required to determine the conditions within the separated-flow region for more exact methods Consequently, figure 10 shows

the dividing-streamline Mach number M_d at the outer corner of the step, both as a function of $M_{1,e}$ and of h/δ_1. The figures indicate that M_d increases as $M_{1,e}$ and h/δ_1 increase. For $M_{1,e} \geq 3$, M_d is supersonic for $h/\delta_1 \geq 4$. For $M_{1,e} = 5$, M_d is supersonic for $h/\delta_1 > 1$. These plots indicate that for many supersonic free-stream Mach numbers and step-height ratios, one should consider the possibility of a normal shock near the step face if accurate pressure distributions are required.

Effect of normal shock.- The effect of a normal shock on the flow is illustrated in figure 11. The most severe practical case for the present range of calculations is considered $\left(M_{1,e} = 6 \text{ and } h/\delta_1 = 10\right)$.

The effect of the normal shock is significant on the pressures near the dividing streamline when the flow is supersonic, but the effect on the integrated drag coefficient C_D is only about 3 percent if the same total pressure loss is assumed in the reverse-flow region as in the shear layer. This error in the drag coefficient is so small that it was not considered necessary to include the normal shock effect in the drag calculations in this report. Due to the normal shock, the static pressure at the step face is drastically changed and is no longer constant. Consequently, the assumption of constant static pressure everywhere behind the oblique shock is not valid with the normal shock present and any attempt to include this variable static pressure in the theory greatly increases the complexity of the calculations.

The largest error $\Delta C_D/C_D$ resulting from negligence of the normal shock effect on C_D occurs at the higher Mach number investigated $\left(M_{1,e} = 6\right)$ and is shown as a function of h/δ_1 in figure 12. The ratio $\Delta C_D/C_D$ is the difference in the integrated drag coefficient with and without a normal shock existing whenever the flow is supersonic. The curve indicates that $\Delta C_D/C_D$ increases rapidly from 0.001 at $h/\delta_1 = 1$ to an asymptotic value of about 0.04 for $h/\delta_1 \geq 100$ Thus, the effect of the normal shock on C_D can be neglected, for the range of conditions covered in this report.

Comparison With Experiment

Pressure distributions.- Because of the great number of simplifications and assumptions involved in the present analysis, the accuracy and usefulness of the theory can only be established by comparison with experiment Confidence in the theory can be enhanced only if it can be shown that the pressure distributions obtained by the theory are in reasonable agreement with experimental ones. Comparisons are presented in figure 13. Inasmuch as the experimental data are known not to have a constant pressure distribution on the step face in the reverse-flow region, the theory is modified at this point with the assumption that the pressures in the reverse-flow region are a mirror image of those in the shear-layer portion of the step face with the focal or turning point located at half the step height. For this special case, the requirements of conservation of mass and energy are

automatically satisfied and the momentums in the two regions are equal although in opposite directions. Consequently, this special case meets much more stringent requirements than the general theory where only conservation of mass is involved.

In general, the theoretical pressure distributions have a reasonable similarity to the experimental ones and are of the correct order of magnitude. The comparison suggests, however, that the assumed separation angles θ_s are too small at all Mach numbers. An increase in θ_s will also tend slightly to improve the agreement in the shapes of the theoretical and experimental curves in the shear-flow region. The experimental data indicate that the pressures in the reverse-flow region are not as high as those in the shear-flow area. This trend suggests that the effective static pressure, due to θ_s, is not constant but decreases with distance from the upper corner of the step. The minimum value in the experimental pressures appears to occur in the general area of $y/h = 0.4$ rather than the value of 0.5 assumed in the theory. Note, finally, that many of the experimental pressure distributions are not truly adequate to determine reliable values of either the dividing-streamline stagnation pressure or step-face drag coefficient.

Reattachment pressures and drag.- A comparison of the theoretical and experimental values of $p_{o,d}/p_1$ and C_D corresponding to the pressure distributions of figure 13 and additional available experimental data are presented in figure 14. Experimental data are taken from references 1 and 5 to 10. Table I presents the relationship between the symbols and basic parameters for the experimental data along with the sources from which the data were obtained. In some cases the extrapolations of some of the experimental data were so large that the $p_{o,d}/p_1$ and C_D values that were determined were considered to be too unreliable to justify plotting. In some instances the experimental C_D values determined from experimental pressures do not match those determined by Uebelhack. In particular, the data of Sterrett and Barber (ref. 5) as presented by Uebelhack appear to be in error. Furthermore, some of Uebelhack's data could not be plotted as a function of h/δ_1 because insufficient information was given for identification.

The comparison indicates that in general the theoretical reattachment pressures are in good agreement with experiment as far as magnitudes of values and trends with Mach number and step-height ratio are concerned. There is some scatter in the experimental data with the data of Uebelhack appearing to be consistently lower than the data from the other sources. The data of Sterrett and Barber also appear to indicate a much more rapid rise in $p_{o,d}/p_1$ with h/δ_1 than predicted by the theory for the higher experimental step-height ratio. More data are required to establish whether this is a true trend or merely an experimental aberration.

The drag results, on the other hand, indicate that the theory tends to generally under-predict the experimental values but predicts the correct variation with Mach number. The theory also probably predicts the correct variation with h/δ_1; however, the experimental

data are too meager and the scatter too large to verify this fact satisfactorily. The inability of the theory to predict the correct magnitude of the drag coefficient is ascribed to the use of too low values of the assumed separation angle θ_s over most of the Mach number range.

In view of the erroneous density relations used to determine $p_{o,d}/p_1$, the improper interpretation of Sterrett and Barber's results, and the incorrect calculated trend with h/δ_1, the agreement between theory and experiment presented by Uebelhack appears to be somewhat fortuitous.

Empirical Extension of Theory to Small Step-Height Ratios

The theory was developed for cases where $h/\delta_1 \geqq 2$, however, there is a great need to develop drag-prediction methods for $h/\delta_1 < 2$. Consequently, an investigation was made to determine the requirements for developing such an extension using some unpublished experimental data together with data from reference 6 as a guide.

The unpublished data (see ref. 11 for some limited results) indicated that the step-face pressures and drags decreased to 0 as h/δ_1 approached 0. Furthermore, the data indicated that both the static pressures due to the separation angle θ_s and the dynamic pressure in the shear layer had to decrease with decreasing h/δ_1. In order to achieve this trend, a decrease in θ_s had to be coupled with an increase in the shear-spreading parameter σ. Obviously, a large number of combinations of θ_s and σ could provide the desired results. In order to keep the calculations orderly, the assumption was made that there was a functional relationship between θ_s and σ and that this relationship could be expressed as

$$\sigma\theta_s = f\left(M_{2,e}\right) \tag{12}$$

The relationship between θ_s and h/δ_1 was assumed to be given by

$$\theta_s = a_0 + a_1\left(\ln\frac{h}{\delta_1}\right) + a_2\left(\ln\frac{h}{\delta_1}\right)^2 + a_3\left(\ln\frac{h}{\delta_1}\right)^3 \tag{13}$$

This expression provided the best fit to the experimental data of the 8 types of expressions investigated. Equation (13) allows θ_s to decrease very slowly at first from the reference value at some chosen value of h/δ_1, then decrease much more rapidly at the lower step-height ratios, and end with a slow decrease in θ_s toward 0 as h/δ_1 tends toward 0. Calculations were then made at $M_{1,e} = 1.61$ to determine the boundary conditions that would fit the empirical curve to the experimental data. These boundary conditions are

Upper boundary conditions.

$$\frac{h}{\delta_1} = 7 \qquad \theta_s = 12.25° \qquad \frac{\partial \theta_s}{\partial\left(h/\delta_1\right)} = 0 \tag{14}$$

Lower boundary conditions·

$$\frac{h}{\delta_1} = 0.004 \qquad \theta_s = 0.004° \qquad \frac{\partial \theta_s}{\partial\left(h/\delta_1\right)} = 0.004 \text{ or } 0.0 \tag{15}$$

The same boundary conditions except for upper θ_s (for which 13.25° was used) were then used to calculate the theoretical curve at $M_{1,e} = 2.2$. The results of all these calculations are shown in figure 15 where both $p_{o,d}/p_1$ and C_D are plotted as functions of h/δ_1. The experimental data are shown in the form of shaded bands. The widths of these bands are primarily due to Reynolds number effects and not scatter. These Reynolds number effects can be readily incorporated into the theory; however, no attempt was made to do so in the present investigation. These experimental Reynolds number effects are considerably larger than the theoretical effects calculated for changes in the index of the power-law velocity profile, and hence suggest then an additional parameter not considered herein may be involved.

Figure 15 shows that, in general, theory is in good agreement with experiment at both Mach numbers. Note that this agreement extends down to h/δ_1 in the order of 0.001 for the drag coefficients despite the fact that the pressure integral (eq. (3)) is singular for $h/\delta_1 = 0$. The experimental data for $p_{o,d}/p_1$ were not plotted to such low values of h/δ_1 because the models had become so small in height that, in the extreme case, only one or two orifices were available to represent the pressure distributions, and pressure peaks could not be isolated. Note also that the experimental data never fall below the static pressure curves and thus appear to confirm a reasonable division between static (θ_s) and dynamic pressure (σ) effects in the extended theory

The value of $h/\delta_1 = 7$ required for the upper boundary condition in matching the theory with experiment may appear to be too high and the possibility exists that the function chosen to relate θ_s to h/δ_1 may be too elementary and the approach of the extended theory to the basic theoretical curves may occur more sharply. Attempts to resolve the problem, however, uncovered just as many reasons why the value may be valid as why the value is too high.

Although the theory appears to be in good agreement with experimental data for h/δ_1 ratios as low as 0.001, recommendations are made that this theory not be applied to h/δ_1

values less than about 0.05 because of the increasing Reynolds number effects, which are not incorporated into the empirical extension of Uebelhack's basic theory.

Finally, a comparison is made of some pressure distributions predicted by the extended theory with some unpublished experimental results obtained at Mach numbers of 1.61 and 2.20 (fig. 16). An effort was made to pick experimental data that was representative of the central regions of the shaded areas in figure 15 and also reasonably close to the relative location of the theoretical lines in the shaded areas. For the results at a Mach number of 2.20, the $R_{\delta 1} = 0.742 \times 10^6$ data correspond more closely to the center regions of the shaded areas and the $R_{\delta 1} = 0.524 \times 10^6$ data relate more closely to the areas next to the theoretical curve in the h/δ_1 range of interest. As before, the theoretical reverse-flow pressures are assumed to be mirror images of those in the shear-layer region. Note that the theoretical and experimental step-height ratios do not coincide exactly.

In general, the agreement between theory and experiment is good. A significant feature indicated by the experimental results is that the reattachment point (or the dividing streamline) does not occur at the upper corner of the step but at some distance below it and that this distance increases as h/δ_1 decreases. Behrens (ref. 7) also notes this effect. What this means is that the shear-layer flow above the reattachment point passes over the top of the step and does not enter the separated-flow region. Consequently, for a more correct comparison with experiment the theoretical region should be foreshortened to include only the distance from the wall to this peak in pressure. Such a foreshortening will substantially improve the agreement between the theoretical and experimental pressure distributions and move the theoretical point of minimum pressure closer to the y/h region of 0.40 to 0.45 where the experimental minimums generally occur. Of importance is the fact that most experimental results do not contain sufficient detail of the pressure distributions near the upper corner, making it difficult to accurately estimate reattachment pressures or face-drag coefficients. Finally, the agreement between theory and experiment would not have been quite as good if no effort had been made to match the data approximately for Reynolds number effects.

Another point of interest revealed by this analysis is that as h/δ_1 decreases the component of pressure contributed by the dynamic pressure decreases much more rapidly than the component contributed by the static pressure rise across the separation shock. Finally, mention should be made of the fact that the static-pressure measurements of Behrens (ref. 7) on the wall ahead of the step and also outside the shear layer indicate that the linear shear layer probably does not exist for $h/\delta_1 < 3$. Thus, it is quite surprising that the extended theory appears to perform so well.

SUMMARY OF RESULTS

A theoretical investigation has been made of the pressure distributions on and drag characteristics of the faces of forward-facing steps immersed in turbulent boundary layers at supersonic speeds Uebelhack's theory was used as a basis for the calculations but the theory was modified and extended, and a different method was used to obtain the solutions. The results of this investigation are summarized as follows

(1) Decreases in the assumed separation angle and increases in the assumed shear-layer spreading parameter result in decreased pressure levels and drag forces, with the separation angle affecting the effective static pressure and the spreading parameter the dynamic pressure in the separated-flow region.

(2) Increases in the index of the assumed power-law velocity profiles caused small increases in the dividing streamline or reattachment pressures at the smaller ratios of step height to boundary-layer thickness but had no significant effect on the drag.

(3) Modification of the theory so that the shear layer always terminates at the center height of the step face and replacement of the rectangular pressure distribution of the reverse flow with the mirror image of the shear flow resulted in increased accuracy in the calculations and in reasonably good agreement between theoretical and experimental face pressure distributions for moderate ratios of step height to boundary-layer thickness (from 2 to 7).

(4) By coupling a decrease in assumed separation angle with an increase in the shear-layer spreading parameter, the modified theory can be extended to give good agreement between theory and experiment to ratios of step height to boundary-layer thickness decreasing to values as low as 0.05 at free-stream Mach numbers of 1.61 and 2.20.

(5) There is some disagreement between the results obtained in this investigation and those of Uebelhack which apparently cannot be ascribed to different methods of computation.

Langley Research Center
National Aeronautics and Space Administration
Hampton, Va. 23665
August 26, 1975

APPENDIX A

THEORY

The primary assumptions in Uebelhack's shear-flow model for boundary-layer separation ahead of a forward-facing step have been mentioned in the section entitled "Theoretical Approach." For details on the secondary assumptions and general development, see reference 1. The main objective herein is to point out some deviations from Uebelhack's approach that were utilized in the present paper and to correct the typographical errors in some equations in reference 1.

Separation Region

The boundary-layer momentum thickness θ_2 behind the oblique shock at the separation point is an important parameter combining mass and momentum flux for the free-mixing region and is calculated as follows (see fig. 17):

The conservation of mass in the boundary layer across the oblique shock is given by

$$\int_0^{\delta_1} \rho_1 u_1 \, dy = \int_0^{\delta_2} \rho_2 u_2 \, dy \tag{A1}$$

The momentum flux across the oblique shock in the x-direction is given by

$$p_1\delta_1 + \int_0^{\delta_1} \rho_1 u_1^2 \, dy = p_2\delta_1 + \int_0^{\delta_2} \rho_2 u_2^2 \, dy \cos \theta_s \tag{A2}$$

The oblique-shock theory is then applied to calculate

$$\frac{\rho_{1,e} u_{1,e}}{\rho_{2,e} u_{2,e}} = \frac{\sin\left(\beta - \theta_s\right)}{\sin \beta} \tag{A3}$$

and

$$\frac{\rho_{1,e} u_{1,e}^2}{\rho_{2,e} u_{2,e}^2} = \frac{p_1 M_{1,e}^2}{p_2 M_{2,e}^2} = \frac{\sin\left(\beta - \theta_s\right)}{\sin \beta} \frac{\cos\left(\beta - \theta_s\right)}{\cos \beta} \tag{A4}$$

APPENDIX A

Introduce the boundary-layer displacement and momentum thicknesses defined by:

$$\delta^* = \int_0^{\delta} \left(1 - \frac{\rho u}{\rho_e u_e}\right) dy \tag{A5}$$

$$\theta = \int_0^{\delta} \frac{\rho u}{\rho_e u_e}\left(1 - \frac{u}{u_e}\right) dy \tag{A6}$$

Use of equations (A3) to (A6) in equations (A1) and (A2) allows the calculation of the boundary-layer momentum thickness as follows:

$$\theta_2 = -\frac{1}{\cos \theta_s}\left[\left(\delta_1 - \delta_1^* - \theta_1\right)\frac{\sin (\beta - \theta_s)}{\sin \beta}\,\frac{\cos (\beta - \theta_s)}{\cos \beta}\right.$$
$$\left. - \left(\delta_1 - \delta_1^*\right)\frac{\sin (\beta - \theta_s)}{\sin \beta}\cos \theta_s + \delta_1 \frac{p_1 - p_2}{\gamma p_2 M_{2,e}^2}\right] \tag{A7}$$

Free-Shear Layer

The shear-layer velocity profile in the mixing region is approximated by the error function profile of the form

$$\frac{u_2}{u_a} = \frac{u_2}{u_{2,e}} = \phi = \frac{1}{2}[1 + \text{erf } (\eta)] \tag{A8}$$

where

$$\text{erf } (\eta) = \frac{2}{\sqrt{\pi}} \int_0^{\eta} e^{-\xi^2}\, d\xi \tag{A9}$$

$$\eta = \frac{\sigma y}{x} \tag{A10}$$

where ξ is a dummy variable.

The spreading factor σ is not known exactly for compressible fluids; Korst and Chow (ref. 2) suggest the following correlation

$$\sigma = 12 + 2\,76 M_{2,e} \tag{A11}$$

APPENDIX A

For the constant stagnation temperature and constant static-pressure flow with unit Prandtl number, Crocco's integral relationship is applicable. In this case, the density ratio is given by

$$\frac{\rho_2}{\rho_a} = \frac{\rho_2}{\rho_{2,e}} = \frac{1 - C_a^2}{1 - C_a^2\phi^2} \tag{A12}$$

As the shear layer grows in the downstream direction from the virtual origin, the origin of the coordinate system, which is anchored to the center of the velocity profile, is displaced toward the lower velocity. The coordinate shift y_m is determined from the continuity and momentum equations using the control volume indicated in figure 18. The continuity equation is

$$-\rho_b u_b y_{rb} + \rho_a u_a y_{ra} + \int_0^x \rho_b v_b \, dx = \int_{y_{rb}+y_m}^{y_{ra}+y_m} \rho u \, dy \tag{A13}$$

The momentum equation is

$$-\rho_b u_b^2 y_{rb} + \rho_a u_a^2 y_{ra} + \int_0^x \rho_b v_b u_b \, dx = \int_{y_{rb}+y_m}^{y_{ra}+y_m} \rho u^2 \, dy \tag{A14}$$

In these equations y_{rb} and y_{ra} are arbitrary large negative and positive values, respectively, such that

$$u\left(y_{ra}\right) \rightarrow u_a = u_{2,e}$$

and

$$u\left(y_{rb}\right) \rightarrow u_b$$

and the integral value does not change significantly for further increases in the limits. After combination of equations (A13) and (A14), normalization with $\rho_a u_a$, and with the setting of $u_b = 0$, the result becomes

$$y_m = y_{ra} - \int_{y_{rb}}^{y_{ra}} \frac{\rho}{\rho_a} \phi^2 \, dy \tag{A15}$$

APPENDIX A

By use of the definition of the equations (A10) and (A12), equation (A15) becomes in nondimensional form

$$\eta_m = \eta_{ra} - \int_{\eta_{rb}}^{\eta_{ra}} \frac{\left(1 - C_a^2\right)\phi^2}{1 - C_a^2\phi^2}\, d\eta \tag{A16}$$

The jet boundary streamline η_j, which separates the original jet from the entrained part of the flow, for this case of rectangular initial velocity distribution can be calculated from the continuity equation (see fig. 18)

$$\rho_a u_a y_{ra} = \int_{y_j}^{y_{ra}+y_m} \rho u \, dy \tag{A17}$$

After partial integration and conversion of the above equation to dimensionless form, it becomes

$$\eta_{ra} - \eta_m = \int_{\eta_j}^{\eta_{ra}} \frac{\left(1 - C_a^2\right)\phi}{1 - C_a^2\phi^2}\, d\eta \tag{A18}$$

With the use of equation (A16), equation (A18) is further rearranged to calculate the jet boundary streamline

$$\int_{\eta_{rb}}^{\eta_j} \frac{\left(1 - C_a^2\right)\phi}{1 - C_a^2\phi^2}\, d\eta = \int_{\eta_{rb}}^{\eta_{ra}} \frac{\left(1 - C_a^2\right)\phi}{1 - C_a^2\phi^2}\, d\eta - \int_{\eta_{rb}}^{\eta_{ra}} \frac{\left(1 - C_a^2\right)\phi^2}{1 - C_a^2\phi^2}\, d\eta \tag{A19}$$

In the absence of a boundary layer, the η_j streamline is identical to the dividing streamline η_d. When an initial boundary layer exists, the dividing streamline must be displaced to lower velocities in the shear layer to allow for the momentum losses in the boundary layer. This effect can be created by injecting a mass flow of zero x-momentum into the shear flow. (See fig. 19.) From the continuity equation, the mass m_{dj} between the jet boundary streamline η_j and the dividing streamline η_d is given in dimensionless form by

$$\frac{\sigma m_{dj}}{\rho_a u_a x^*} = \int_{\eta_{rb}}^{\eta_j} \frac{\left(1 - C_a^2\right)\phi}{1 - C_a^2\phi^2}\, d\eta - \int_{\eta_{rb}}^{\eta_d} \frac{\left(1 - C_a^2\right)\phi}{1 - C_a^2\phi^2}\, d\eta \tag{A20}$$

Note that the location of the dividing streamline relative to the boundary streamline is defined only by the continuity equation; the momentum equation is not taken into account. This approximation is reasonable for the small mass bleeds involved. The dividing streamline is obtained from the conservation of mass and momentum in the control volume of figure 19. It is found to be

$$\int_{\eta_{rb}}^{\eta_d} \frac{\left(1 - C_a^2\right)\phi}{1 - C_a^2\phi^2}\, d\eta = -\frac{\sigma\theta_2}{x^*} + \int_{\eta_{rb}}^{\eta_{ra}} \frac{\left(1 - C_a^2\right)\phi\left(1 - \phi\right)}{1 - C_a^2\phi^2}\, d\eta \tag{A21}$$

where θ_2 is the boundary-layer momentum thickness.

Due to the injection of the air in the shear layer, the shear layer is thickened. Hence the virtual origin is moved ahead of the actual separation point along the center line of the shear layer (fig. 20). Thus the length of the shear layer is increased in the system by the amount x_o (from that without boundary layer), and the new length of the shear layer $\bar{x}$ is given by

$$\bar{x} = x^* + x_o \tag{A22}$$

The analysis for calculation of the length x_o is shown below.

The term $\sigma\theta_2/x^*$ determines η_d in momentum equation (A21) and the term $\sigma m_{dj}/\rho_a u_a x^*$ determines η_d in continuity equation (A20), so that simultaneous solution of the two equations gives

$$m_{dj} = \rho_a u_a \theta_2 \tag{A23}$$

The mass m_{dj} can be considered to be injected and entrained between $x = 0$ and $x = x_o$. Hence

$$m_{dj} = \int_0^{x_o} \rho_b v_b\, dx = \rho_b v_b x_o \tag{A24}$$

APPENDIX A

From equations (A23) and (A24), x_o can be related to θ_2

$$\frac{x_o}{\theta_2} = \frac{\rho_a u_a}{\rho_b v_b} = \frac{1}{1 - C_a^2} \frac{u_a}{v_b} \tag{A25}$$

Also, for the control volume of figure 19, the continuity equation is used to determine the injected mass below the jet boundary streamline η_j Thus, another expression for x_o is obtained

$$\frac{x_o}{\theta_2} = \frac{\sigma}{\int_{\eta_{rb}}^{\eta_j} \frac{\left(1 - C_a^2\right)\phi}{1 - C_a^2\phi^2} \, d\eta} \tag{A26}$$

For the new arrangement, a new dimensionless lateral distance $\bar{\eta}$ is defined as $y\sigma/\bar{x}$ and the same theory as for the shear layer without injection is utilized. The dividing-streamline location in the barred $\bar{\eta}$ coordinate system is obtained from equation (A21) as

$$\int_{\bar{\eta}_{rb}}^{\bar{\eta}_d} \frac{\left(1 - C_a^2\right)\phi}{1 - C_a^2\phi^2} \, d\bar{\eta} = - \frac{\sigma\theta_2}{\bar{x}} + \int_{\bar{\eta}_{rb}}^{\bar{\eta}_{ra}} \frac{\left(1 - C_a^2\right)\phi\left(1 - \phi\right)}{1 - C_a^2\phi^2} \, d\bar{\eta} \tag{A27}$$

where the integral limits $\bar{\eta}_{ra}$ and $\bar{\eta}_{rb}$ are arbitrary numbers sufficiently large so as not to affect the value of the integral significantly. The integral value, hence, will not change by changing the limits η_{ra} and η_{rb} to $\bar{\eta}_{ra}$ and $\bar{\eta}_{rb}$ For actual calculations, the integral on the right side of equation (A27) is replaced by the term $\sigma\theta_2/x_o$ which can be calculated in the original unbarred coordinate system from the following equation derived from equations (A26) and (A19)

$$\int_{\bar{\eta}_{rb}}^{\bar{\eta}_{ra}} \frac{\left(1 - C_a^2\right)\phi\left(1 - \phi\right)}{1 - C_a^2\phi^2} \, d\bar{\eta} = \int_{\bar{\eta}_{rb}}^{\bar{\eta}_j} \frac{\left(1 - C_a^2\right)\phi}{1 - C_a^2\phi^2} \, d\bar{\eta} = \int_{\eta_{rb}}^{\eta_j} \frac{\left(1 - C_a^2\right)\phi}{1 - C_a^2\phi^2} \, d\eta = \frac{\sigma\theta_2}{x_o} \tag{A28}$$

APPENDIX A

Reattachment Region

The point of reattachment of the dividing streamline is assumed fixed at the outer corner of the step. Because of the adjustment of the shear layer for the initial boundary-layer thickness, the dividing streamline no longer hits the corner of the step as originally assumed. Consequently, the new location of $\bar{\eta}_d$ has to be found by iteration until the dividing streamline meets the corner of the step within the desired accuracy.

The impingement point of the dividing streamline on the step face is usually initially located below the corner by the distance $\Delta\eta$ (see fig. 21). This distance can be reduced to zero by the equation (derived from the geometry of fig. 20)

$$\Delta\bar{x} = \Delta\bar{\eta}\,\frac{\bar{x}}{\sigma}\,\tan\theta_s \tag{A29}$$

where

$$\Delta\bar{\eta} = \bar{\eta}_m - \bar{\eta}_d$$

for the first iteration and

$$\Delta\bar{\eta} = \bar{\eta}_{d(old)} - \bar{\eta}_{d(new)}$$

for subsequent iterations. Similarly, the longitudinal distance $\bar{x}$ is computed for each iteration from

$$\bar{x}_{new} = \bar{x}_{old} + \Delta\bar{x} \tag{A30}$$

A new value of η_d that is closer to but still not at the step corner is, of course, calculated from equation (A28) each time a new value of $\bar{x}$ becomes available. The iteration process is continued until $\Delta\bar{\eta}$ becomes insignificantly small in relation to the step height.

The Mach number M_d on the dividing streamline is given by

$$M_d^2 = \frac{2}{\gamma - 1}\,\frac{C_a^2\phi_d^2}{1 - C_a^2\phi_d^2} \tag{A31}$$

Uebelhack calculated the reattachment stagnation pressure $p_{o,d}$ for this streamline by the isentropic one-dimensional flow equation, where $M_d < 1$

$$\frac{p_{o,d}}{p_1} = \frac{p_{o,d}}{p_2}\frac{p_2}{p_1} = \left(1 + \frac{\gamma - 1}{2} M_d^2\right)^{\frac{\gamma}{\gamma-1}} \frac{p_2}{p_1} \tag{A32}$$

and by Rayleigh's formula when $M_d > 1$. The method of calculation of $p_{o,d}/p_1$ for subsonic M_d is not correct, because the flow is stagnated by the isentropic process at the step face whereas the assumption has already been made that the flow in the shear layer has constant static pressure and constant total temperature. For $M_d > 1$ there is insufficient information given to make a comment at this point. For the correct method of calculating the desired pressure ratio some additional derivations are required, hence the method will be discussed later.

Reverse-Flow Region

The shear-layer flow and the reverse-flow regions are shown in figure 22. The height of the shear layer below the dividing streamline is AB and AE is the vertical total distance for the reverse-flow region. The distance AB is given by

$$AB = \left(\bar{\eta}_d - \bar{\eta}_{rb}\right)\frac{\bar{x}}{\sigma} \tag{A33}$$

and the distance AE is given by

$$AE = h - AB \cos\theta_s = h - \left(\bar{\eta}_d - \bar{\eta}_{rb}\right)\frac{\bar{x}}{\sigma}\cos\theta_s \tag{A34}$$

The mass flows through AB and AE are assumed equal. With this assumption, the reverse-flow velocity can be found from (with the reverse-flow velocity assumed uniform)

$$\frac{u_b}{u_a} = \frac{1}{1 - C_a^2}\int_{\bar{\eta}_{rb}}^{\bar{\eta}_d} \frac{\left(1 - C_a^2\right)\phi}{1 - C_a^2\phi^2}\, d\bar{\eta}\, \frac{1}{\frac{\sigma h}{\bar{x}} - \left(\bar{\eta}_d - \bar{\eta}_{rb}\right)\cos\theta_s} \tag{A35}$$

With the velocities and densities now known in the region near the step face, the momentum equation can be applied to the control volume shown in figure 19. Lines AB

and AE are assumed close to the step face so that the shear term can be neglected. After some manipulation and simplification, the stagnation pressure integral becomes

$$\int_D^C \frac{p - p_2}{\gamma M_{2,e}^2 p_2}\, dy = \int_A^B \frac{\rho_2 u_2^2}{\rho_a u_a^2}\, dy \cos\theta_s + \int_E^A \frac{\rho_b u_b^2}{\rho_a u_a^2}\, dy \tag{A36}$$

The expressions for the density ratios ρ_2/ρ_a and ρ_b/ρ_a are substituted from equation (A12) and u_b/u_a is substituted from equation (A35) into the equation (A36) to yield

$$\int_0^1 \frac{p - p_2}{p_2}\frac{dy}{h} = \gamma M_{2,e}^2 \frac{\bar{x}}{\sigma h}\left\{\int_{\bar{\eta}_{rb}}^{\bar{\eta}_d} \frac{\left(1 - C_a^2\right)\phi^2}{1 - C_a^2\phi^2}\, d\bar{\eta} \cos\theta_s \right.$$

$$\left. + \frac{1}{1 - C_a^2}\left[\int_{\bar{\eta}_{rb}}^{\bar{\eta}_d} \frac{\left(1 - C_a^2\right)\phi}{1 - C_a^2\phi^2}\, d\bar{\eta}\right]^2 \frac{1}{\frac{\sigma h}{\bar{x}} - \left(\bar{\eta}_d - \bar{\eta}_{rb}\right)\cos\theta_s}\right\} \tag{A37}$$

The pressure integral is related to the free-stream static pressure p_1 existing ahead of the separation shock by

$$\int_0^1 \frac{p}{p_1}\frac{dy}{h} = \left(\int_0^1 \frac{p - p_2}{p_2}\frac{dy}{h} + 1\right)\frac{p_2}{p_1} \tag{A38}$$

The drag coefficient on the step face is calculated from

$$C_D = \frac{\int_0^1 \frac{p}{p_1}\frac{dy}{h} - 1}{\frac{1}{2}\gamma M_{1,e}^2} \tag{A39}$$

APPENDIX A

The correct dividing-streamline pressure is calculated by the use of right first term of equation (A37) after the removal of the integral sign which yields

$$\frac{p_{o,d} - p_2}{p_2} = \gamma M_{2,e}^2 \left[\frac{\left(1 - C_a^2\right)\phi_d^2}{1 - C_a^2 \phi_d^2} \right] \cos \theta_s \tag{A40}$$

and

$$\frac{p_{o,d}}{p_1} = \left(\frac{p_{o,d} - p_2}{p_2} + 1 \right) \frac{p_2}{p_1} \tag{A41}$$

Moreover, the stagnation pressure distribution anywhere through the shear layer below dividing streamline (i.e., along AB) can be calculated from equations (A40) and (A41) by changing ϕ_d to ϕ and $p_{o,d}$ to p. The Mach number along the shear-layer line AB is calculated by

$$M_2^2 = \frac{2}{\gamma - 1} \frac{C_a^2 \phi^2}{1 - C_a^2 \phi^2} \tag{A42}$$

When the free-stream Mach number and h/δ_1 are sufficiently large, a part of the shear layer in AB is supersonic. For this case the flow was decelerated through a normal shock with the stagnation pressure behind the shock being found by using the well-known Rankine-Hugoniot relationships (ref. 4).

APPENDIX B

CALCULATION PROCEDURES

The calculation begins with the specification of δ_1, h, $M_{1,e}$, and n. With M_1 as the entering variable, the separation angle θ_s is found from figure 1 in reference 1. From θ_s, the shock angle β, the Mach number behind the shock, and the static pressure rise p_2/p_1 can be found from tables such as those in reference 4. Two other required quantities δ_1^* and θ_1 can be found in terms of the ratios δ_1^*/δ_1 and θ_1/δ_1 from tables in reference 12 as functions of $M_{1,e}$ and the power of the velocity profile. Finally, the spreading factor σ is calculated from equation (A11) in appendix A and the Crocco number C_a is determined with the aid of equation (51) of reference 4 utilizing the Mach number behind the separation shock as the reference condition.

With all the required basic quantities now known, the next step is to calculate θ_2 by equation (A7), η_m by equation (A16), and η_j by equation (A19) In equation (A19), η_j is a variable upper limit in the integral in the left-hand side of the equation whose value must be found to satisfy the values of the two integrals on the right-hand side. For the present calculations, the limits η_{ra} and η_{rb} were chosen as 3.5 and −1.5, respectively, and calculations indicated that the values of integrals involving these limits were not affected significantly by changes in these limits provided that the changes were in the range $|\eta_{ra}|$ or $|\eta_{rb}| \geqq 1.5$. With the use of η_j, the value of x_o is calculated from equation (A26) and thence the value of $\bar{x}$ from equation (A22) This value of $\bar{x}$ is then introduced into equation (A27) to determine the initial value of $\bar{\eta}_d$. The final value of $\bar{\eta}_d$ is found by iteration with the use of equations (A29) and (A30) to find a new value of $\bar{x}$ which is reintroduced into equation (A27) to find a new value of $\bar{\eta}_d$. The iteration is continued until $\bar{\eta}_d$ is established within the limit of desired accuracy. Finally, with $\bar{\eta}_d$ known, the pressure integral is computed with the aid of equations (A37) and (A38) and the drag coefficient from equation (A39). Note that this procedure does not allow for the existence of any normal shock within the separated-flow region.

The procedures for calculating additional items of interest such as M_d, $p_{o,d}/p_1$, and pressure distribution are quite straightforward and are not detailed here.

The calculation time for a typical run which might include 8 step-height ratios at 5 Mach numbers for a total of 40 points at moderate step-ratios (0.5 to 10) was on the order of 200 sec CPU on the Control Data 6400 computer system.

REFERENCES

1. Uebelhack, H. T.. Theoretical and Experimental Investigation of Turbulent Supersonic Separated Flows Over Front Steps. Vortrag Nr. 71-076, 4th Jahrestag DGLR, Oct. 1971.

2. Korst, H. H.; and Chow, W L · Non-Isoenergetic Turbulent (Pr_t = 1) Jet Mixing Between Two Compressible Streams at Constant Pressure. NASA CR-419, 1966.

3. Birch, Stanley F ; and Eggers, James M.: A Critical Review of the Experimental Data for Developed Free Turbulent Shear Layers. Free Turbulent Shear Flows. Vol I – Conference Proceedings. NASA SP-321, 1972, pp 11-40.

4. Ames Research Staff: Equations, Tables, and Charts for Compressible Flow NACA Rep. 1135, 1953. (Supersedes NACA TN 1428.)

5 Sterrett, James R.; and Barber, John B.: A Theoretical and Experimental Investigation of Secondary Jets in a Mach 6 Free Stream With Emphasis on the Structure of the Jet and Separation Ahead of the Jet. Presented at the Separated Flows Specialists Meeting, Fluid Dynamics Panel (Brussels, Belgium), AGARD, May 9-11, 1966.

6 Lord, Douglas R , and Czarnecki, K. R.: Aerodynamic Loadings Associated With Swept and Unswept Spoilers on a Flat Plate at Mach Numbers of 1.61 and 2.01. NACA RM L55L12, 1956.

7. Behrens, Wilhelm· Separation of a Supersonic Turbulent Boundary Layer by a Forward Facing Step AIAA Paper No. 71-127, Jan. 1971.

8. Vas, I. E.; and Bogdonoff, S. M.: Interaction of a Turbulent Boundary Layer With a Step at M = 3.85. Rep. No. 295 (AFSOR TN 55-200), Dept. Aeronaut. Eng., Princeton Univ., Apr 1955.

9. Hahn, Jerry S. Experimental Investigation of Turbulent Step-Induced Boundary-Layer Separation at Mach Numbers 2 5, 3, and 4. AEDC-TR-69-1, U.S. Air Force, Mar. 1969. (Available from DDC as AD 683 767.)

10. Bogdonoff, Seymour M., and Kepler, C. Edward The Separation of a Supersonic Turbulent Boundary Layer. Preprint No. 441, S.M.F. Fund Paper, Inst. Aeronaut. Sci., Inc., Jan. 25-29, 1954.

11. Czarnecki, K R.: The Problem of Roughness Drag at Supersonic Speeds NASA TN D-3589, 1966.

12 Tucker, Maurice: Approximate Calculation of Turbulent Boundary-Layer Development in Compressible Flow. NACA TN 2337, 1951

TABLE I.- RELATION BETWEEN SYMBOLS AND REFERENCES FOR EXPERIMENTAL DATA OF FIGURE 14

Author	Ref.	$M_{1,e}$	$\frac{h}{\delta_1}$	$\frac{p_{o,d}}{p_1}$	C_D	Symbols in fig. –	
						14(a)	14(b)
H. T. Uebelhack	1	2.0	2.0	3.2		□	□
		3.6	4.0	5.8	0.314	◇	◺
		3.7	4.0	5.6		◇	◺
		3.75		5.8	.305		◺
		4.0		6.3			◺
		4.8	1.5	7 0	.273	○	◺
J. R. Sterrett and J. B. Barber	5	6.0	1.085	10.3	0 238	○	◺
		6.0	1.75	11.4	.2595	□	◺
		6.0	2.42	14.0		□	◺
		6.0	3.08	22.8		◇	◺
D. R. Lord and K. R. Czarnecki	6	1.61	1.3	2.105	0.518	○	○
		1.61	2.0	2.25	544	□	○
		2.01	1.3	2 62	.44	○	□
		2.01	2.0	2.82	.462	□	□
J. S. Hahn	9	2 5	7.14	4.7	0.459	◇	◇
		3.0	5.88	11.4	.4048	◇	△
		3 99	3.7	6.1	.383	◇	◺
I. E. Vas and S. M. Bogdonoff	8	3.85	1.46	7.5	0.3207	○	◺
S. M. Bogdonoff and C. E. Kepler	10	3.0	1.7647	5.1	0.3969	□	△
Wilhelm Behrens	7	3.987	4 035	6.9	0.3145	◇	◺

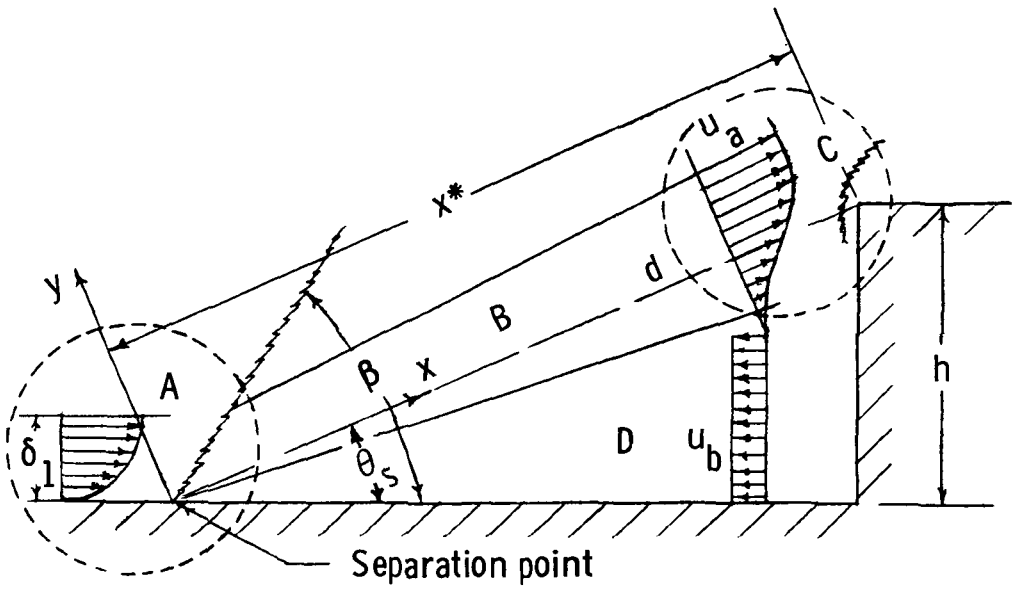

A Separation region
B Free-mixing region
C Reattachment region
D Reverse-flow region

Figure 1.- Basic flow model and subregions.

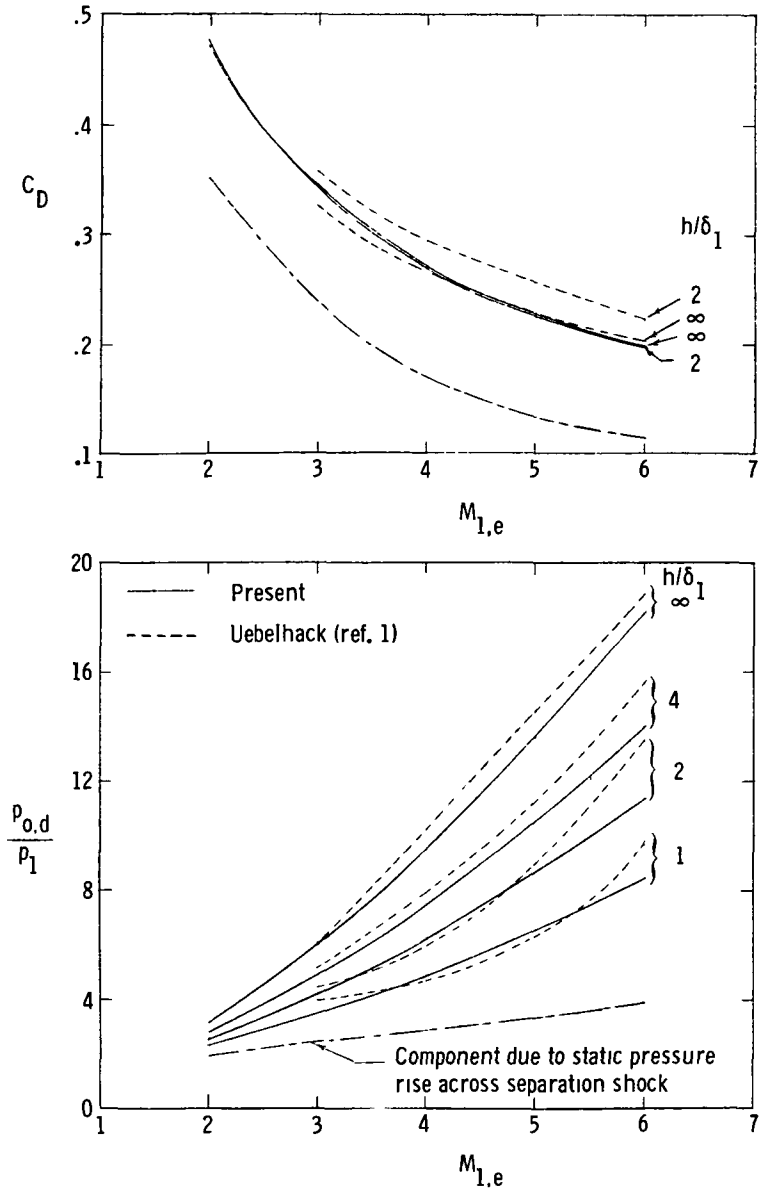

(a) $p_{0,d}/p_1$ and C_D as a function of $M_{1,e}$.

Figure 2.- Comparison of present results with those of Uebelhack. Constant η_{rb}.

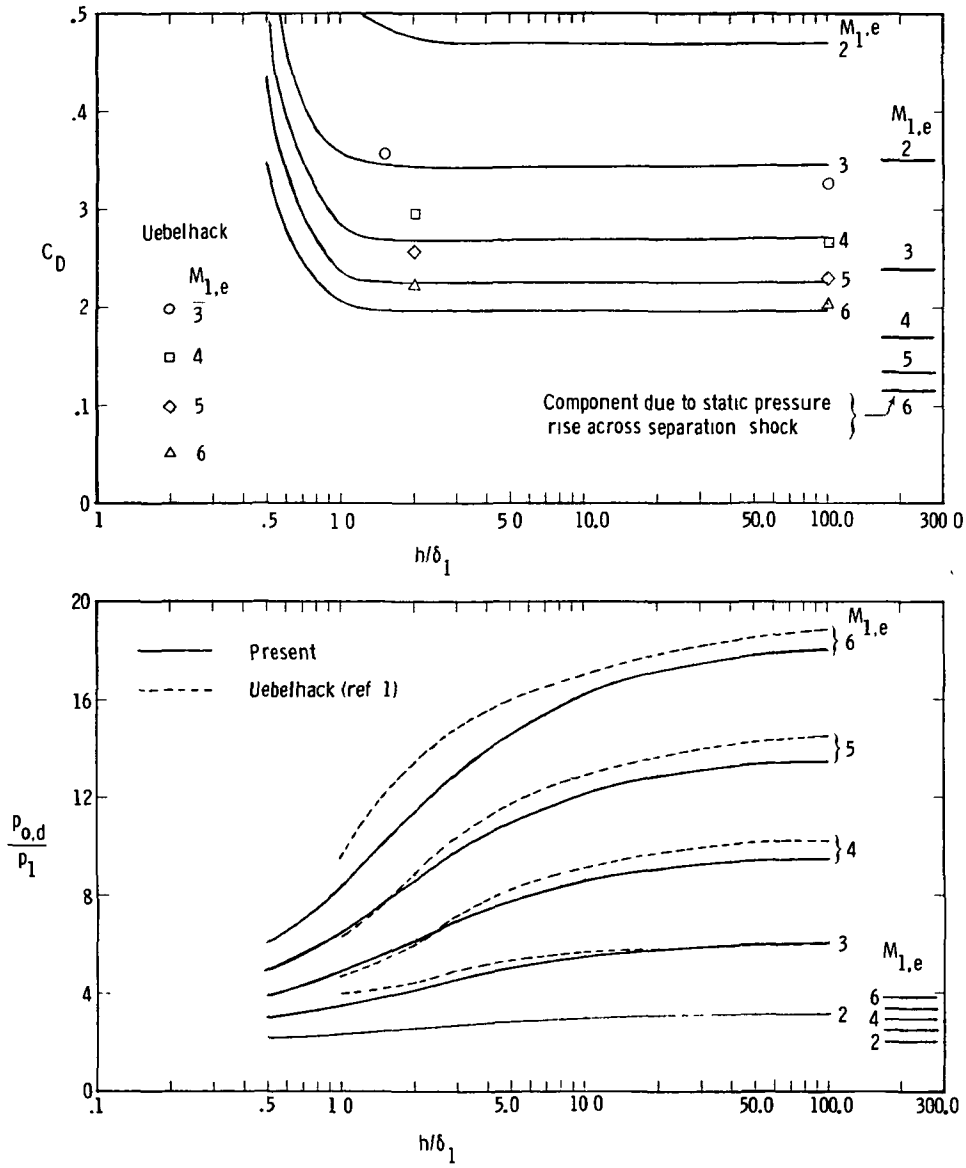

(b) $p_{o,d}/p_1$ and C_D as a function of h/δ_1.

Figure 2.- Concluded.

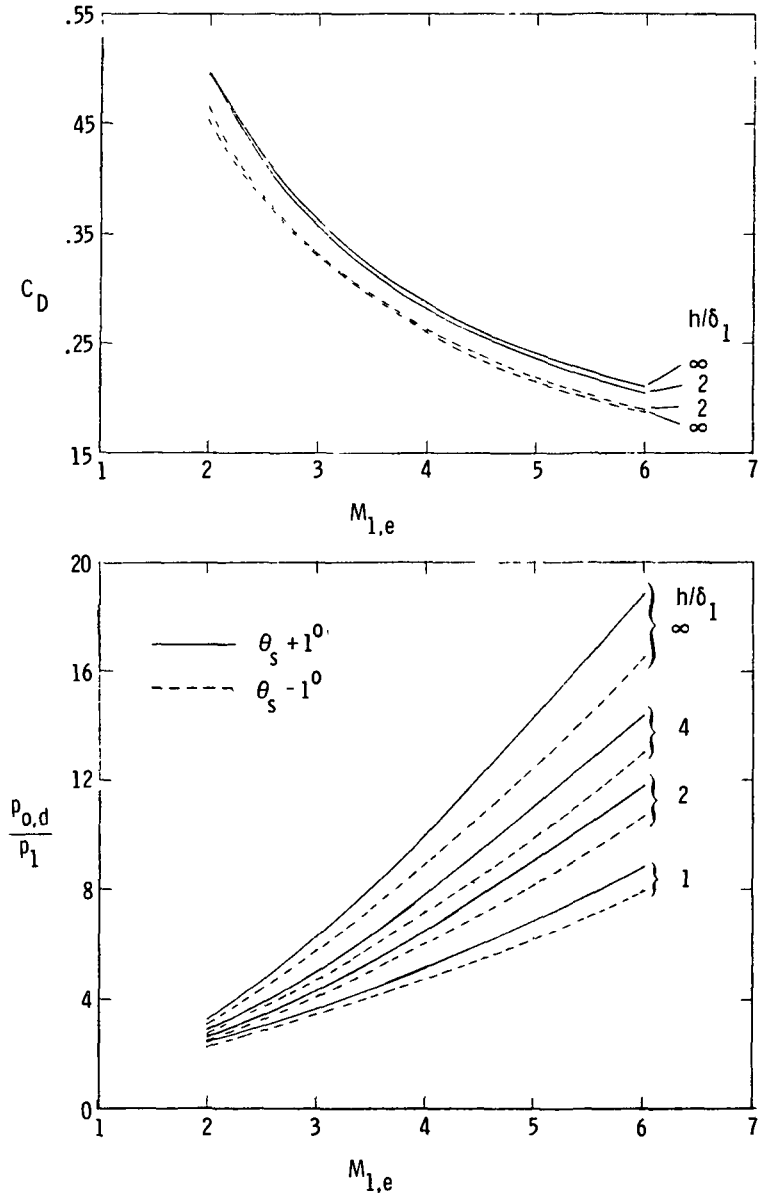

(a) $p_{o,d}/p_1$ and C_D as a function of $M_{1,e}$.

Figure 3.- Effects of changes in θ_s on $p_{o,d}/p_1$ and C_D. Constant η_{rb}.

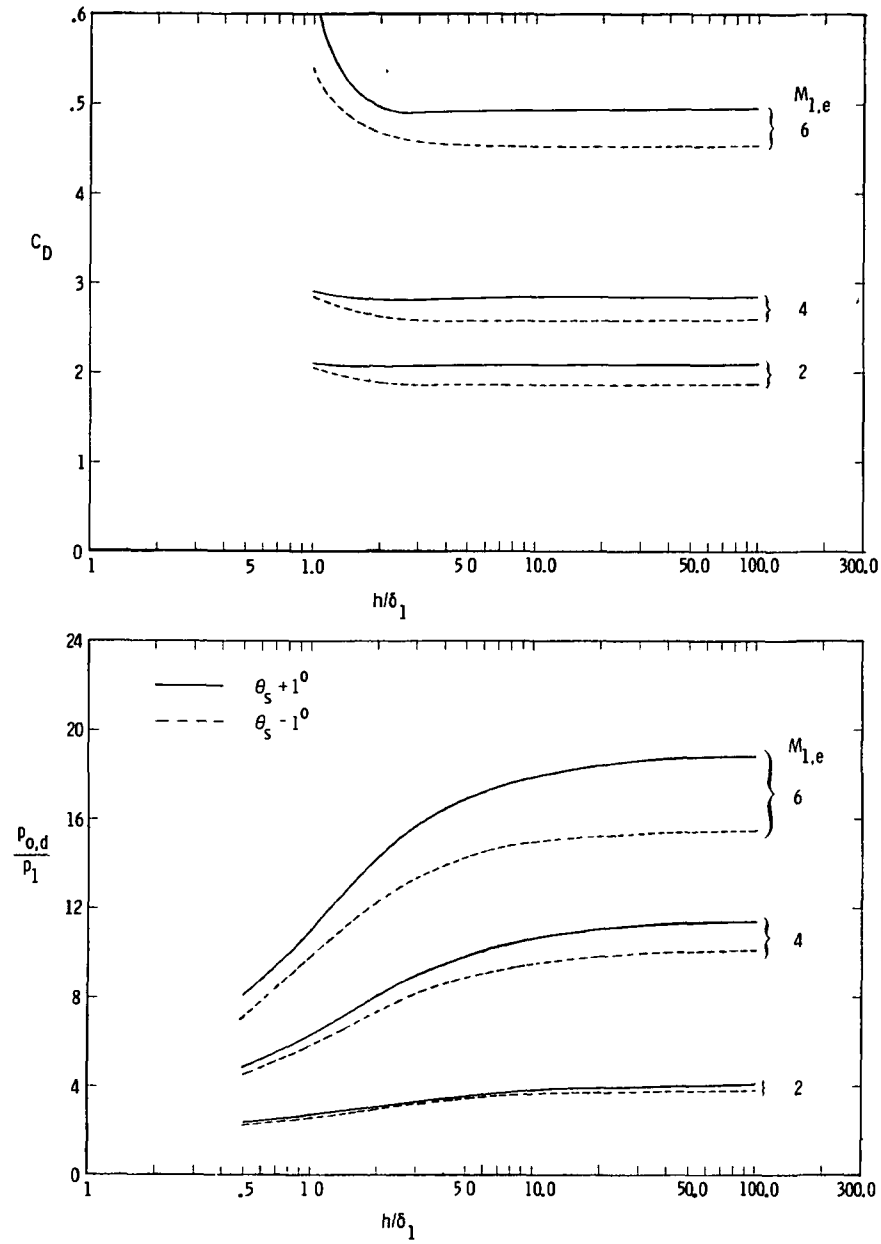

(b) $p_{o,d}/p_1$ and C_D as a function of h/δ_1.

Figure 3.- Concluded.

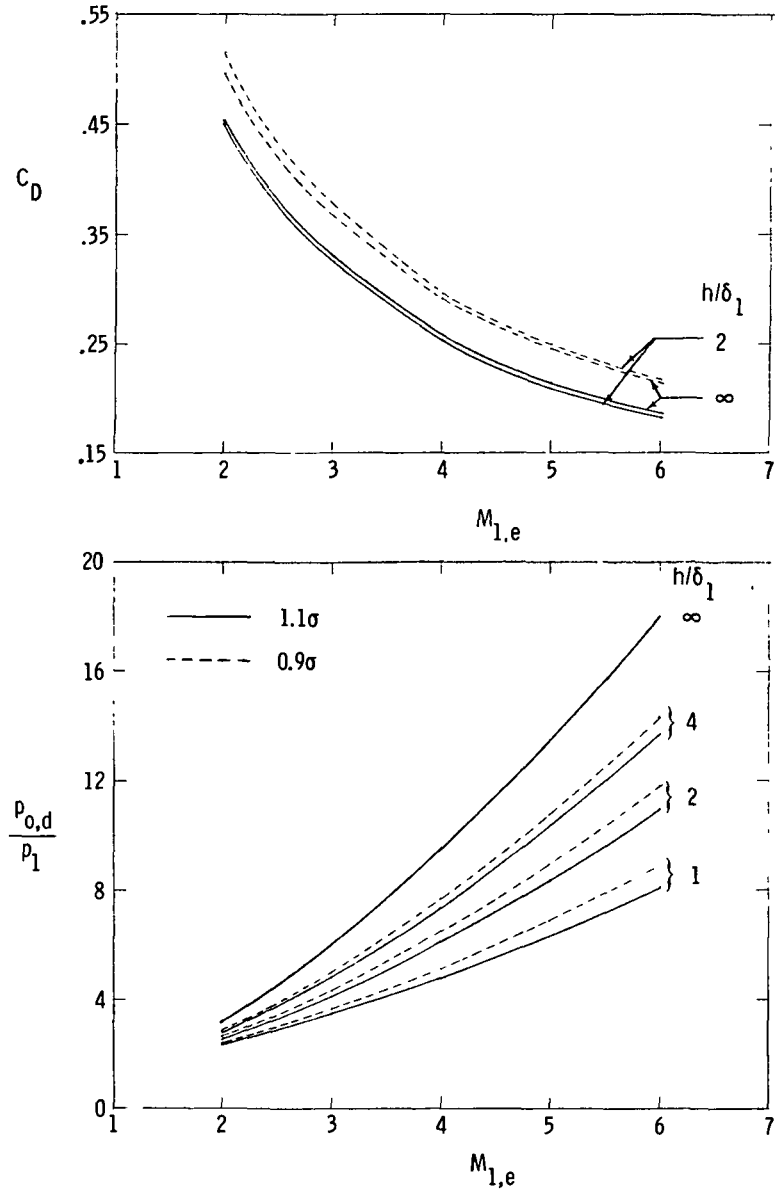

(a) $p_{o,d}/p_1$ and C_D as a function of $M_{1,e}$.

Figure 4.- Effects of changes in σ on $p_{o,d}/p_1$ and C_D. Constant η_{rb}.

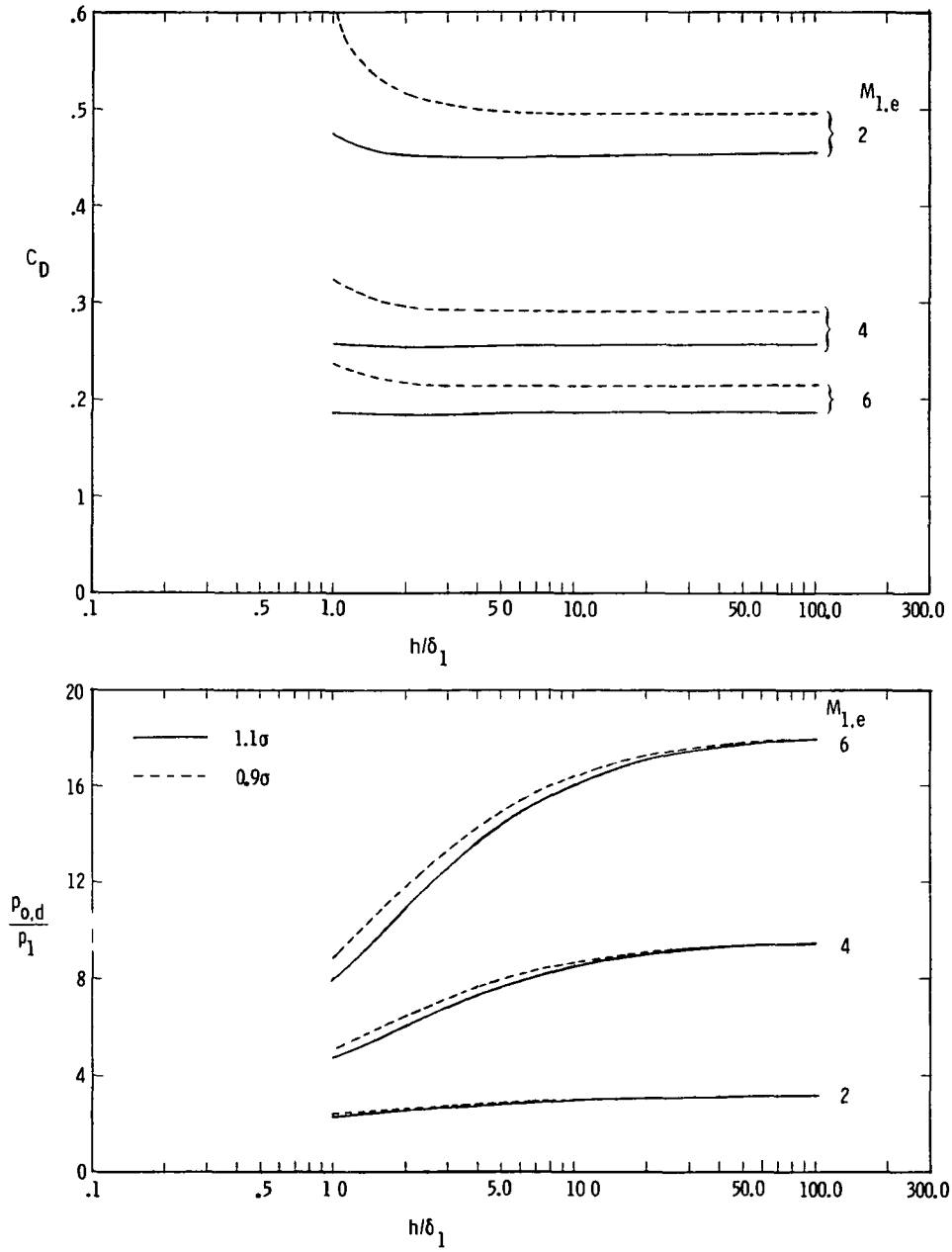

(b) $p_{o,d}/p_1$ and C_D as a function of h/δ_1.

Figure 4.- Concluded.

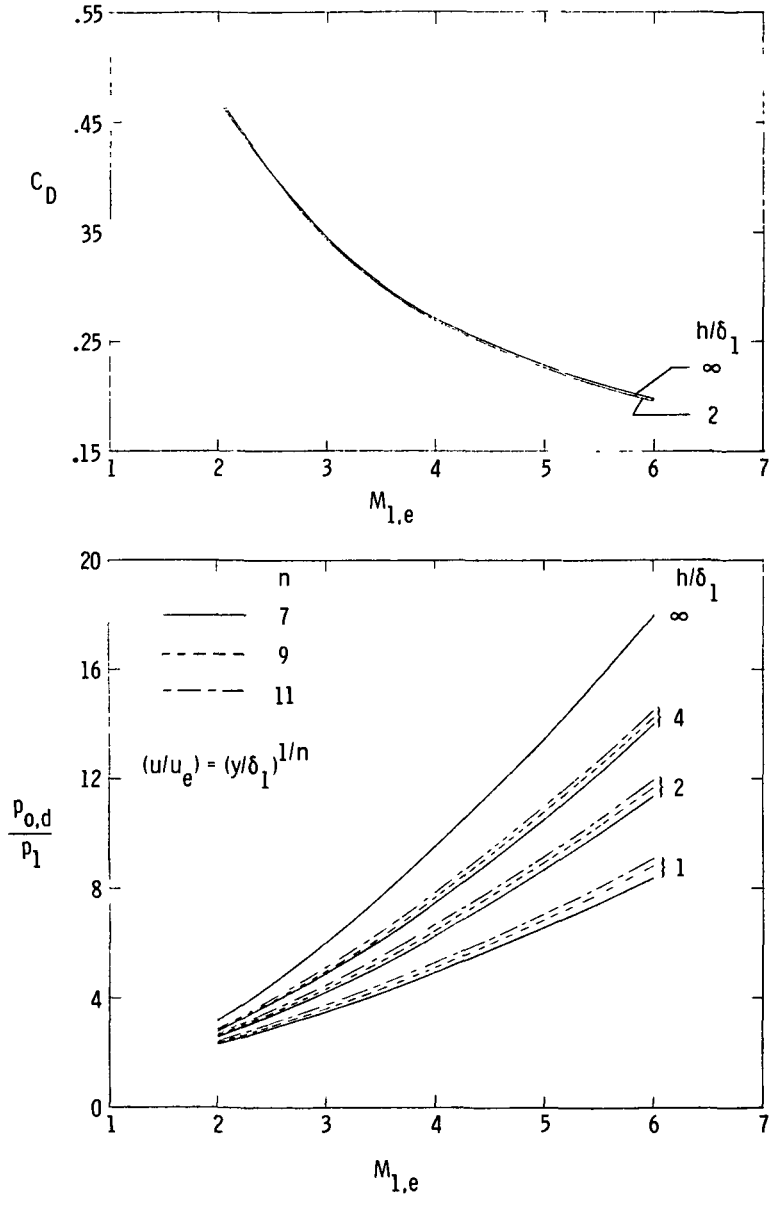

(a) $p_{o,d}/p_1$ and C_D as a function of $M_{1,e}$.

Figure 5.- Effects of changes in velocity profile power-law index. Constant η_{rb}.

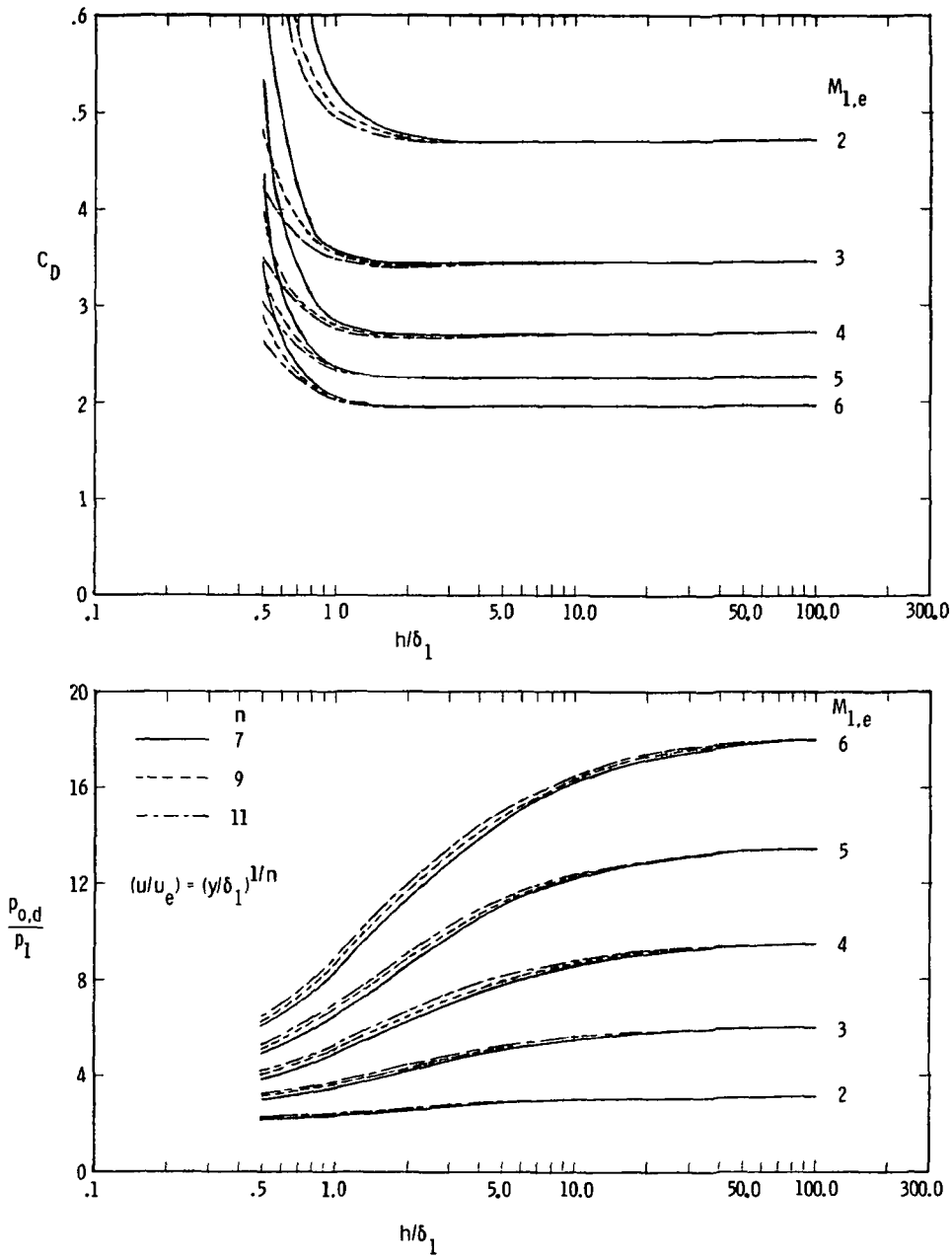

(b) $p_{o,d}/p_1$ and C_D as a function of h/δ_1.

Figure 5.- Concluded.

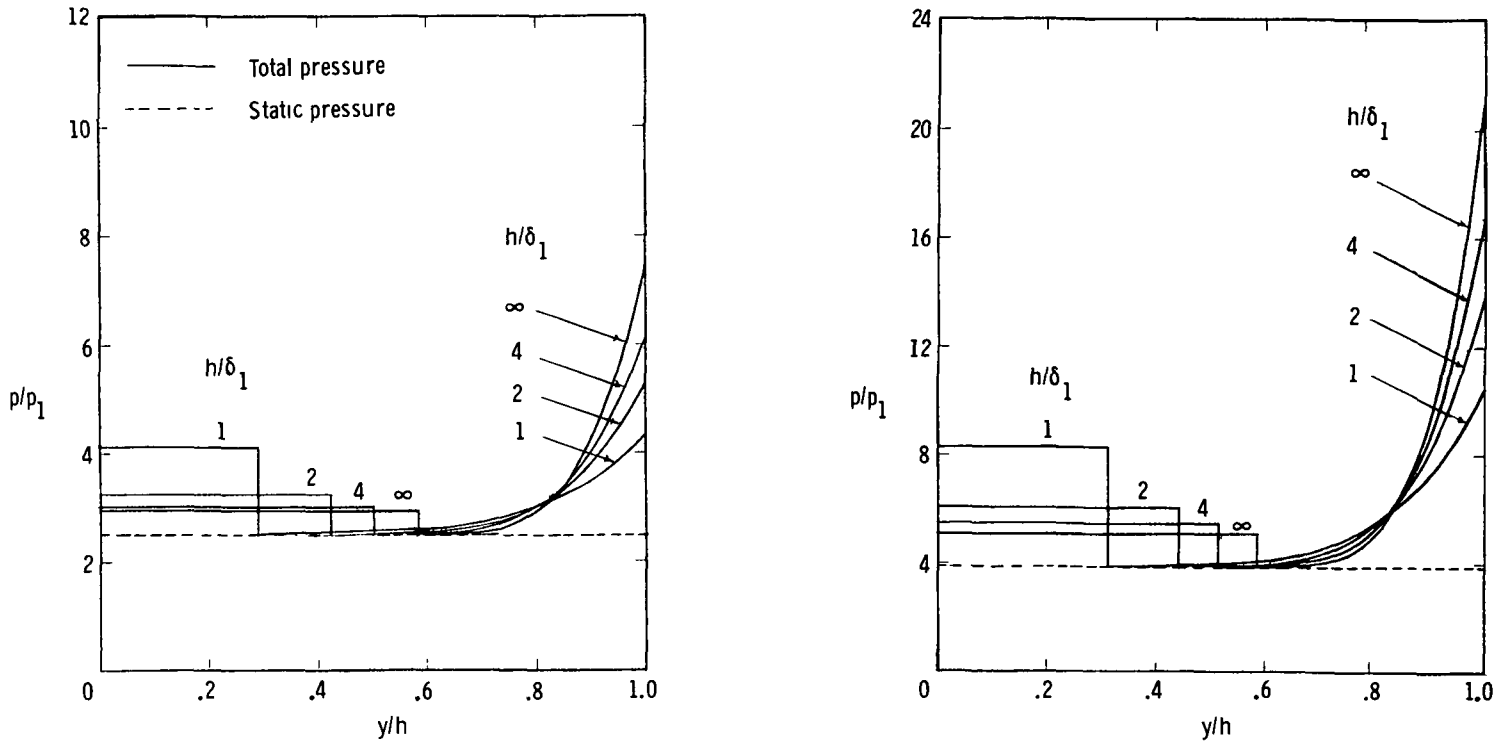

(a) $M_{1,e} = 3$.

(b) $M_{1,e} = 6$.

Figure 6.- Typical effective pressure distribution. Constant η_{rb}; no normal shock.

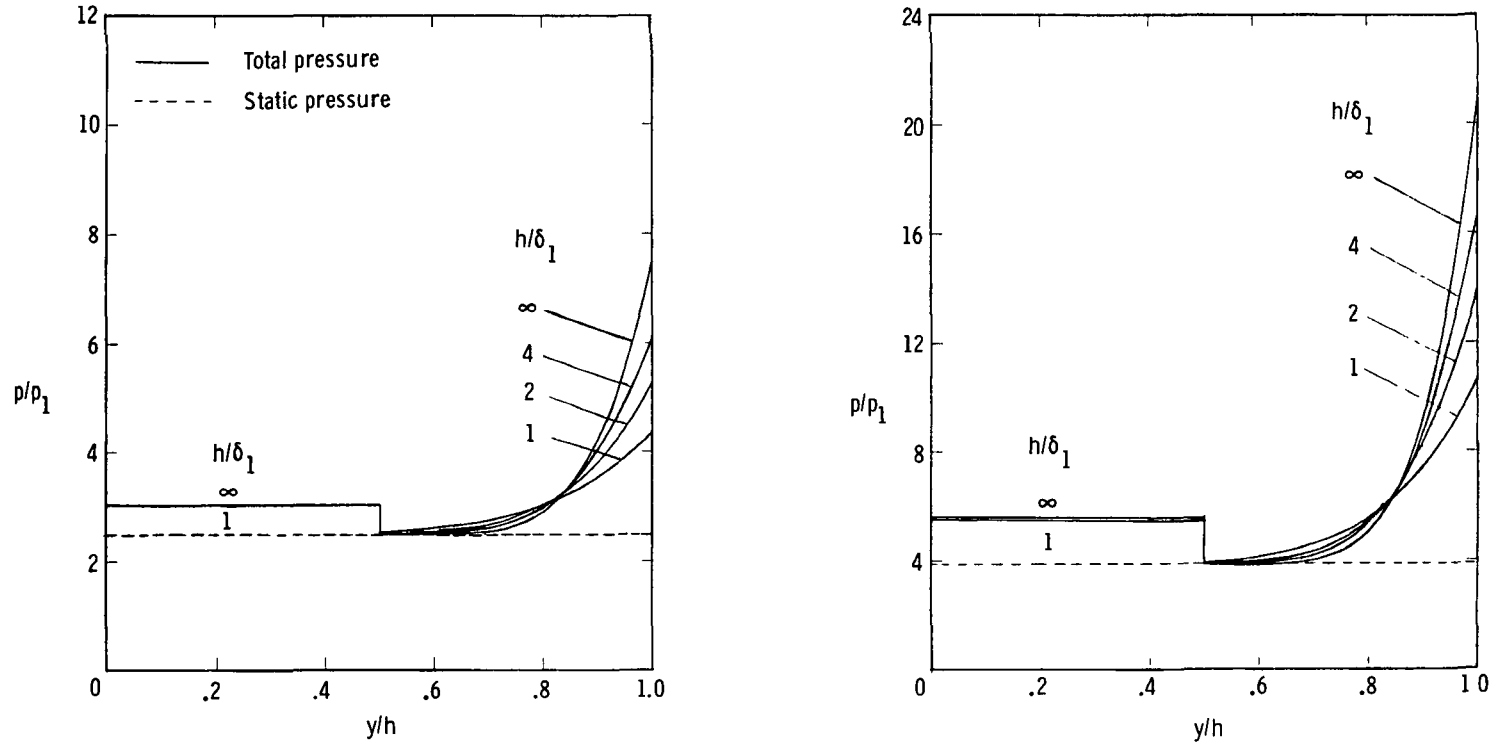

(a) $M_{1,e} = 3.$

(b) $M_{1,e} = 6.$

Figure 7.- Typical effective pressure distribution. Variable η_{rb}; no normal shock.

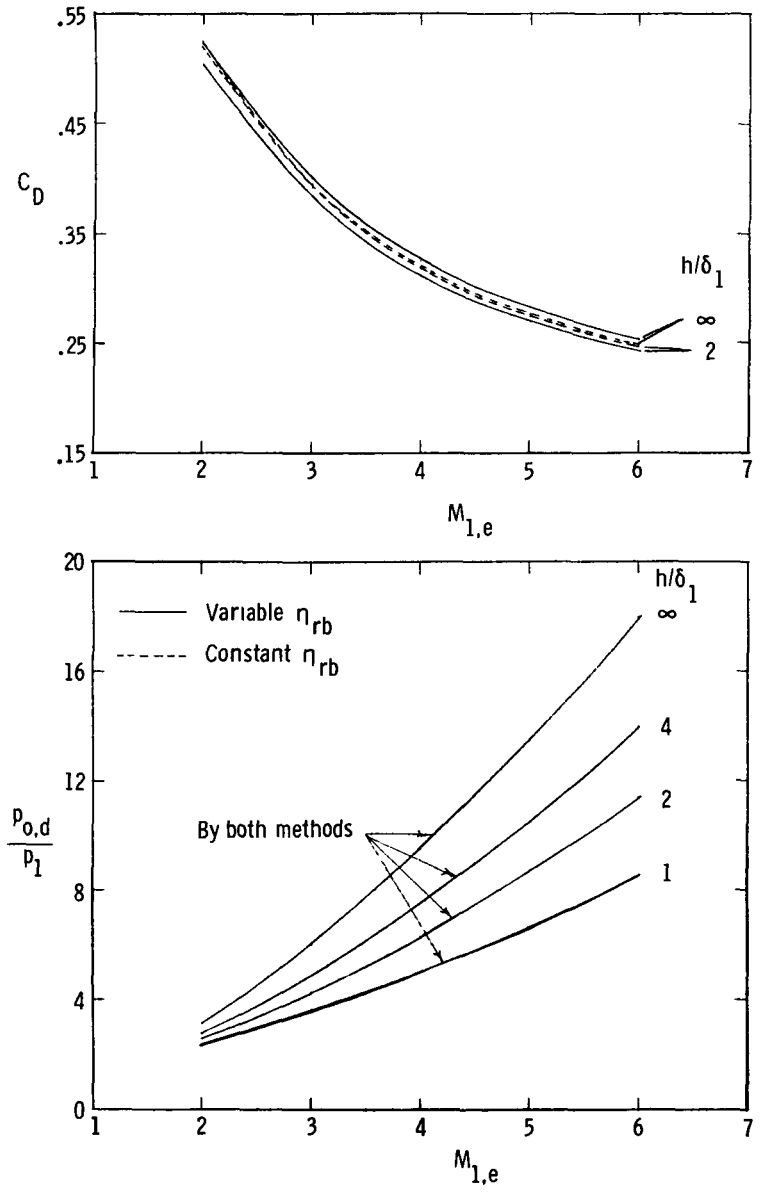

(a) $p_{o,d}/p_1$ and C_D as a function of $M_{1,e}$.

Figure 8.- Comparison of results computed by constant and variable η_{rb} methods.

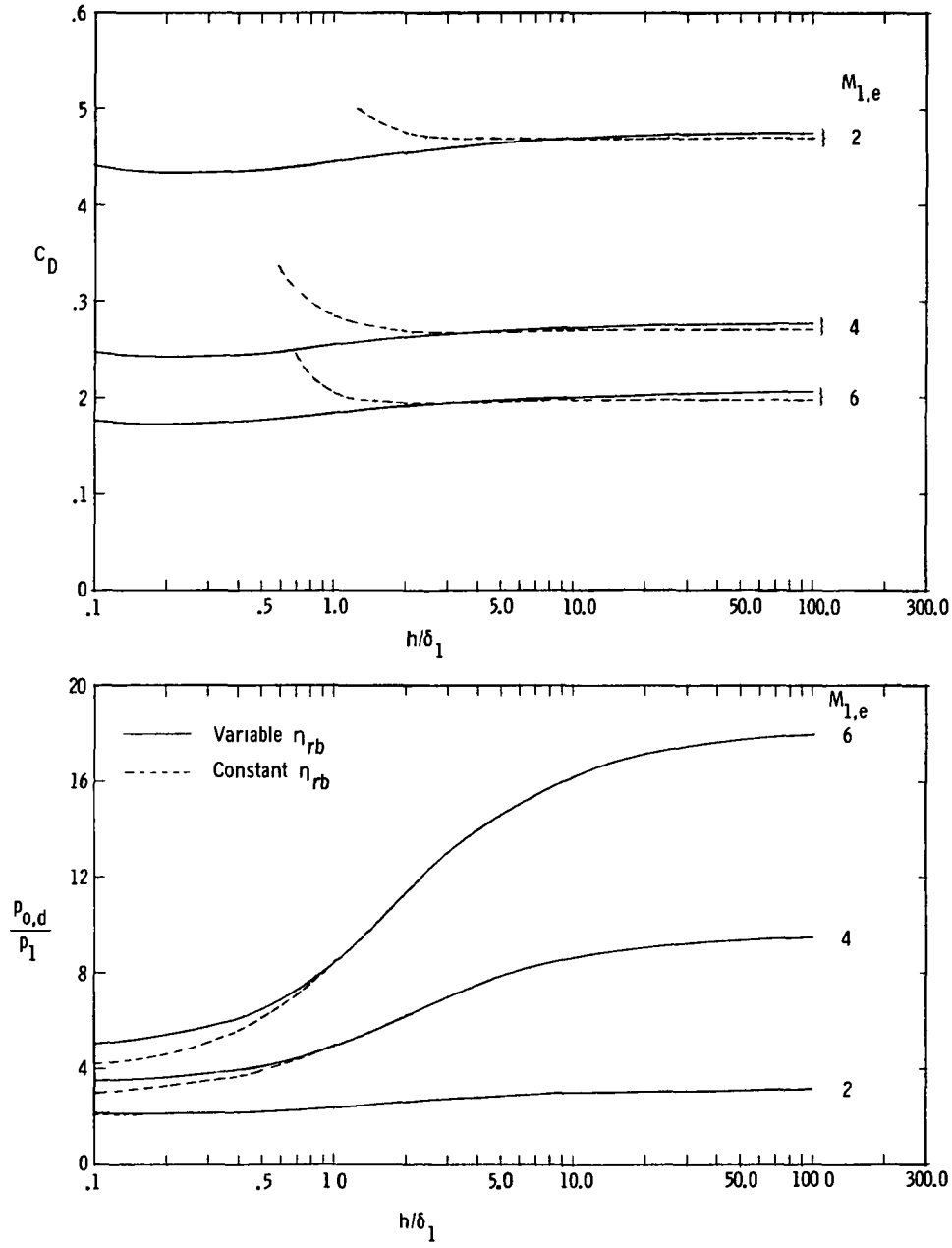

(b) $p_{o,d}/p_1$ and C_D as a function of h/δ_1.

Figure 8.- Concluded.

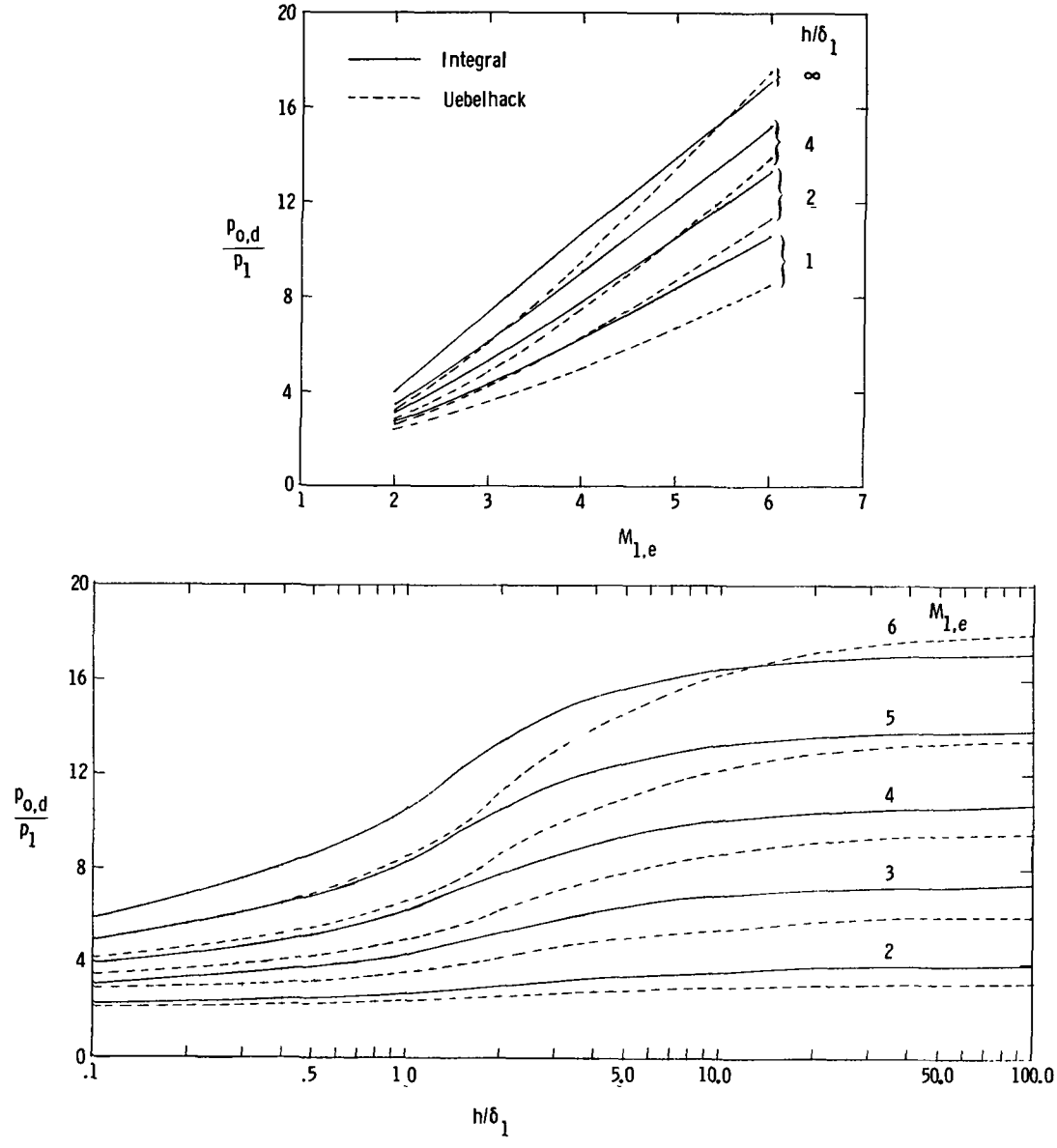

Figure 9.- Comparison of reattachment pressures calculated from equation (7) (integral method) with the present results calculated from equation (6) (Uebelhack's method). Variable η_{rb}.

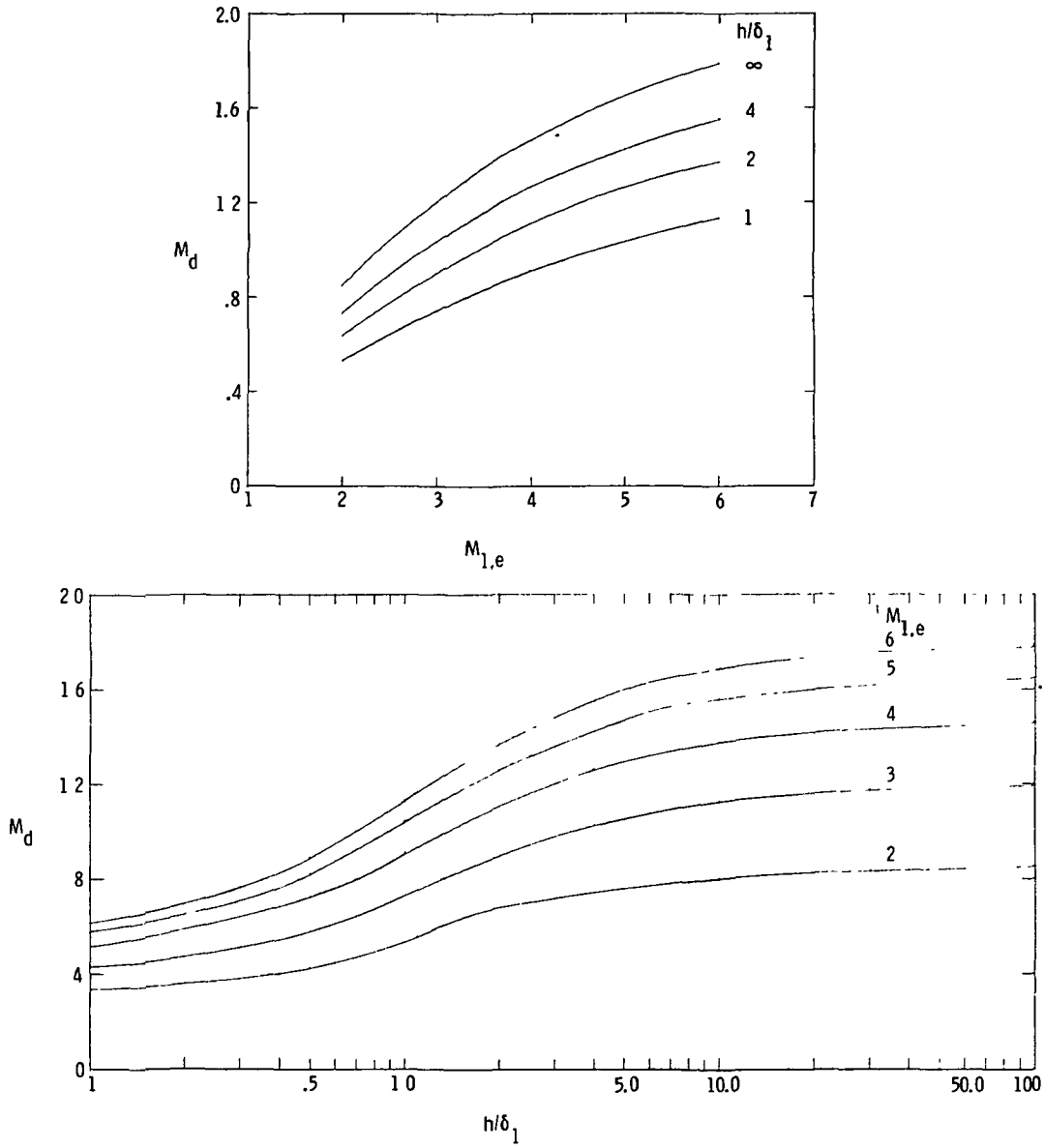

Figure 10.- Variation of dividing-streamline Mach number with $M_{1,e}$ and h/δ_1. Variable η_{rb}.

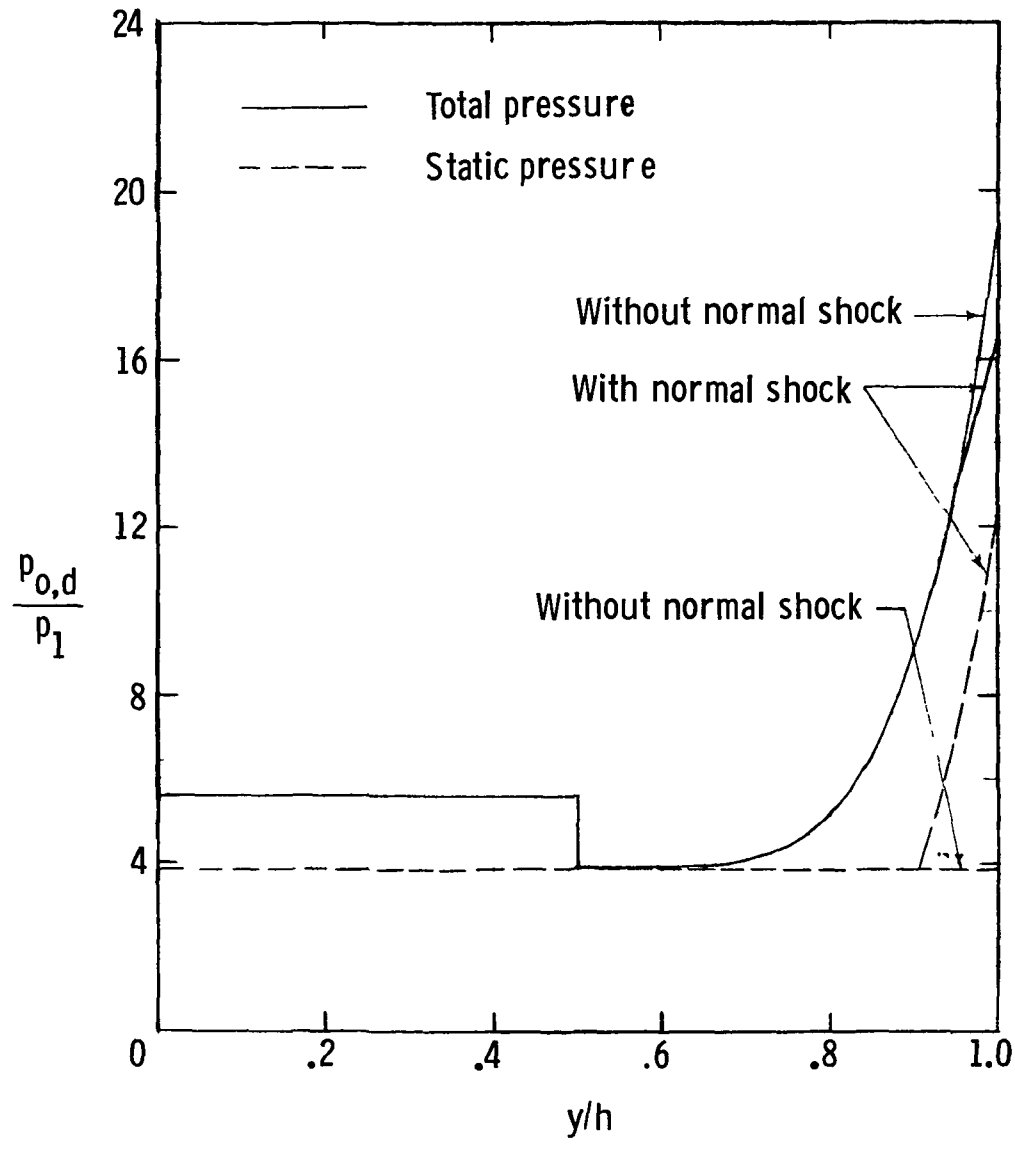

Figure 11.- Pressure distributions on step face with and without normal shock. $M_{1,e} = 6$, $h/\delta_1 = 10$; variable η_{rb}.

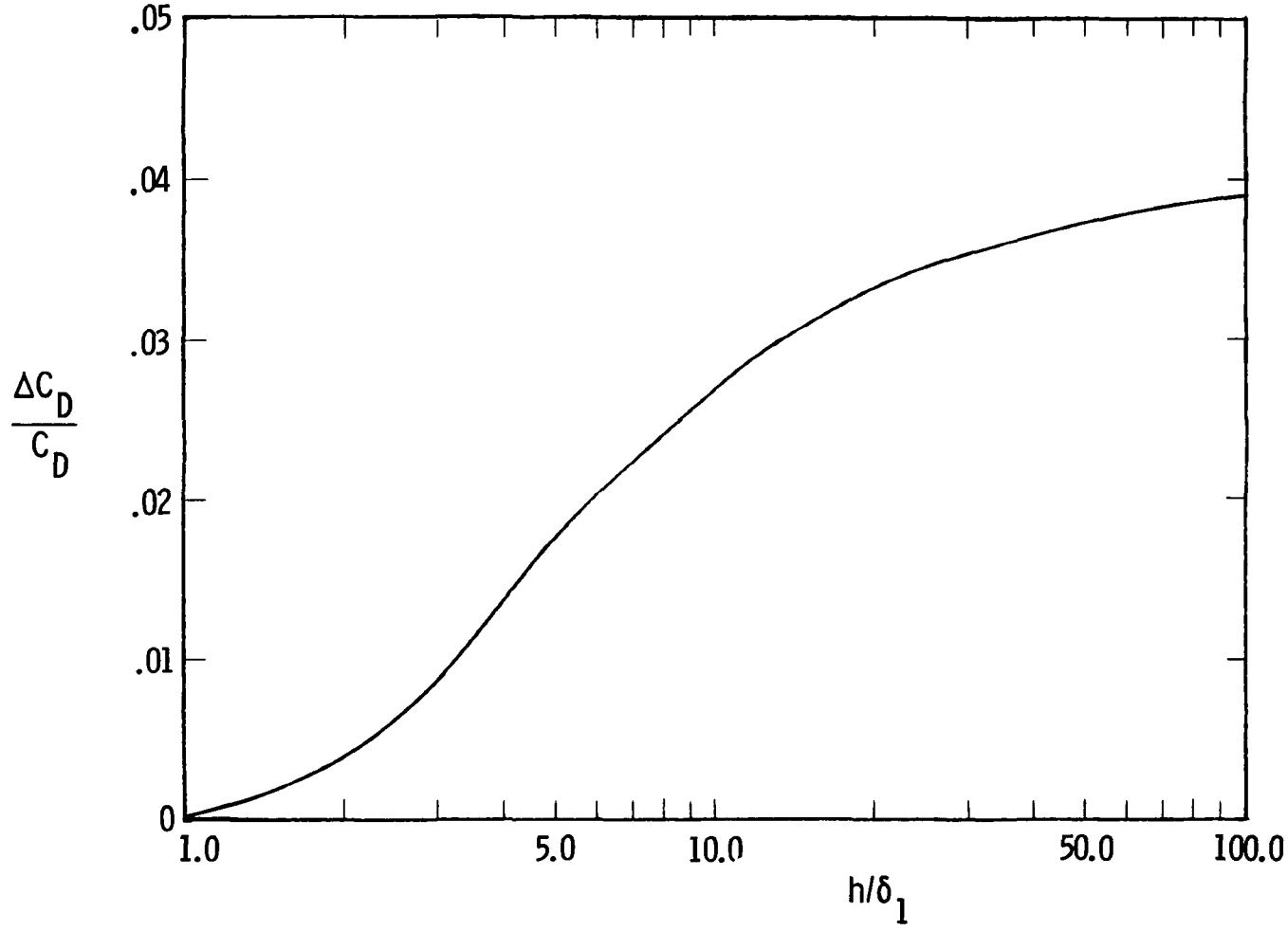

Figure 12.- Variation of $\Delta C_D/C_D$ with h/δ_1. $M_{1,e} = 6$; variable η_{rb}.

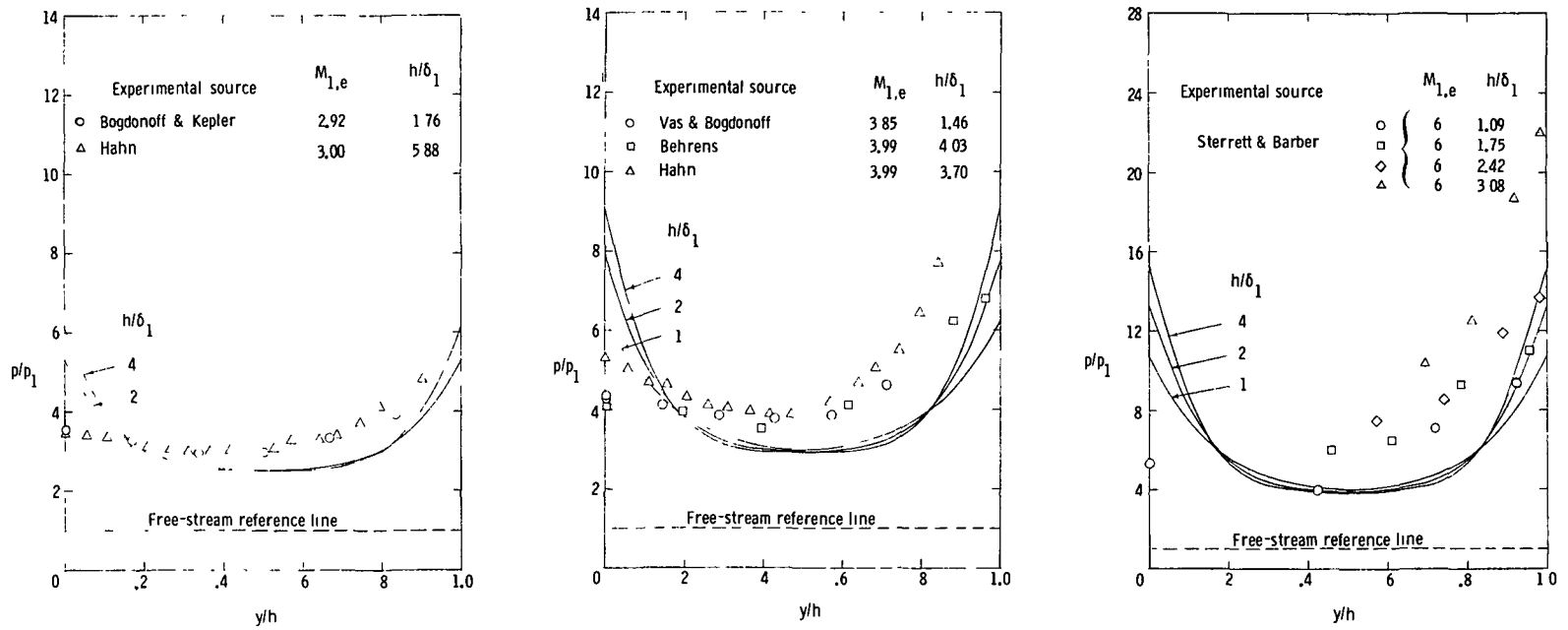

(a) $M_{1,e} = 3$. (b) $M_{1,e} = 4$. (c) $M_{1,e} = 6$.

Figure 13.- Comparison of theoretical and experimental pressure distributions. Variable η_{rb}.

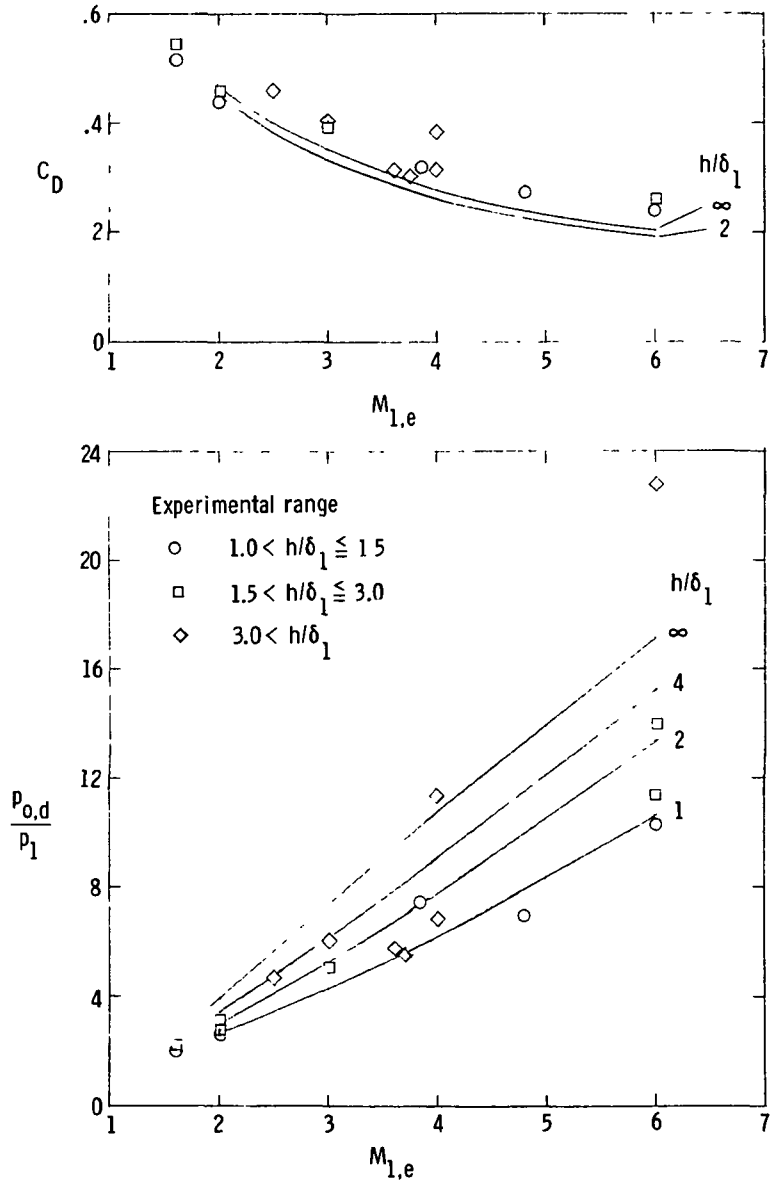

(a) $p_{o,d}/p_1$ and C_D as a function of $M_{1,e}$.

Figure 14.- Comparison of theoretical and experimental values of $p_{o,d}/p_1$ and C_D. Variable η_{rb}.

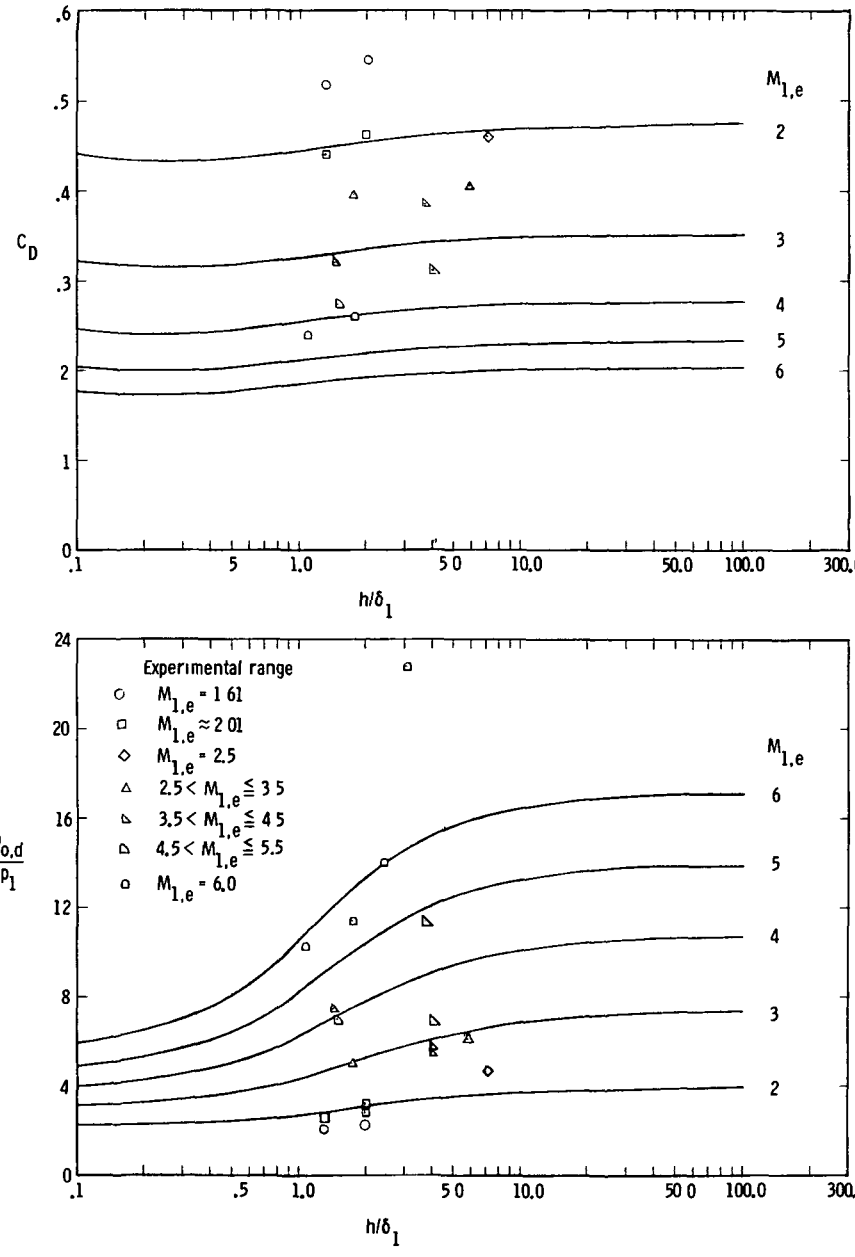

(b) $p_{o,d}/p_1$ and C_D as a function of h/δ_1.

Figure 14.- Concluded.

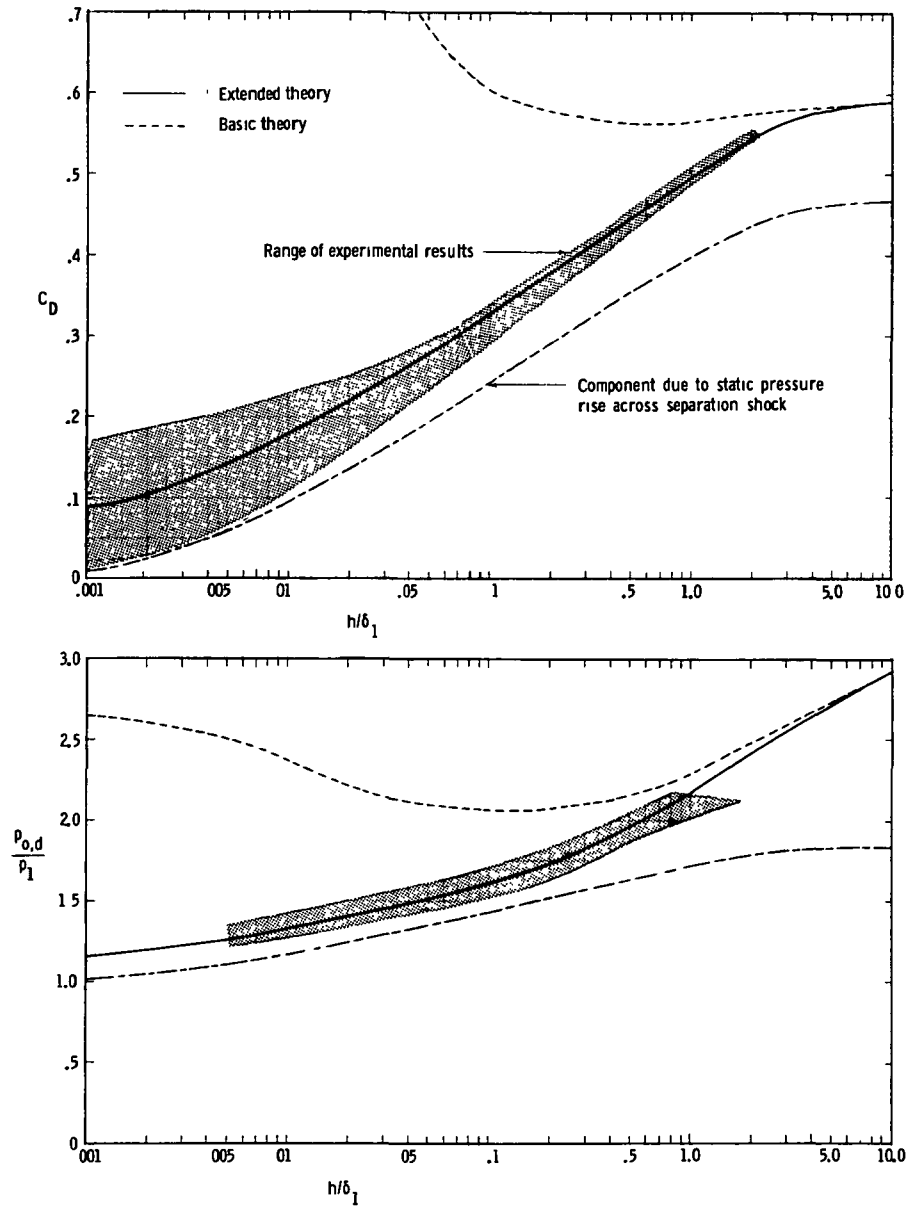

(a) $M_{1,e} = 1.61$.

Figure 15.- Comparison of extended theory with experiment. Variable η_{rb}.

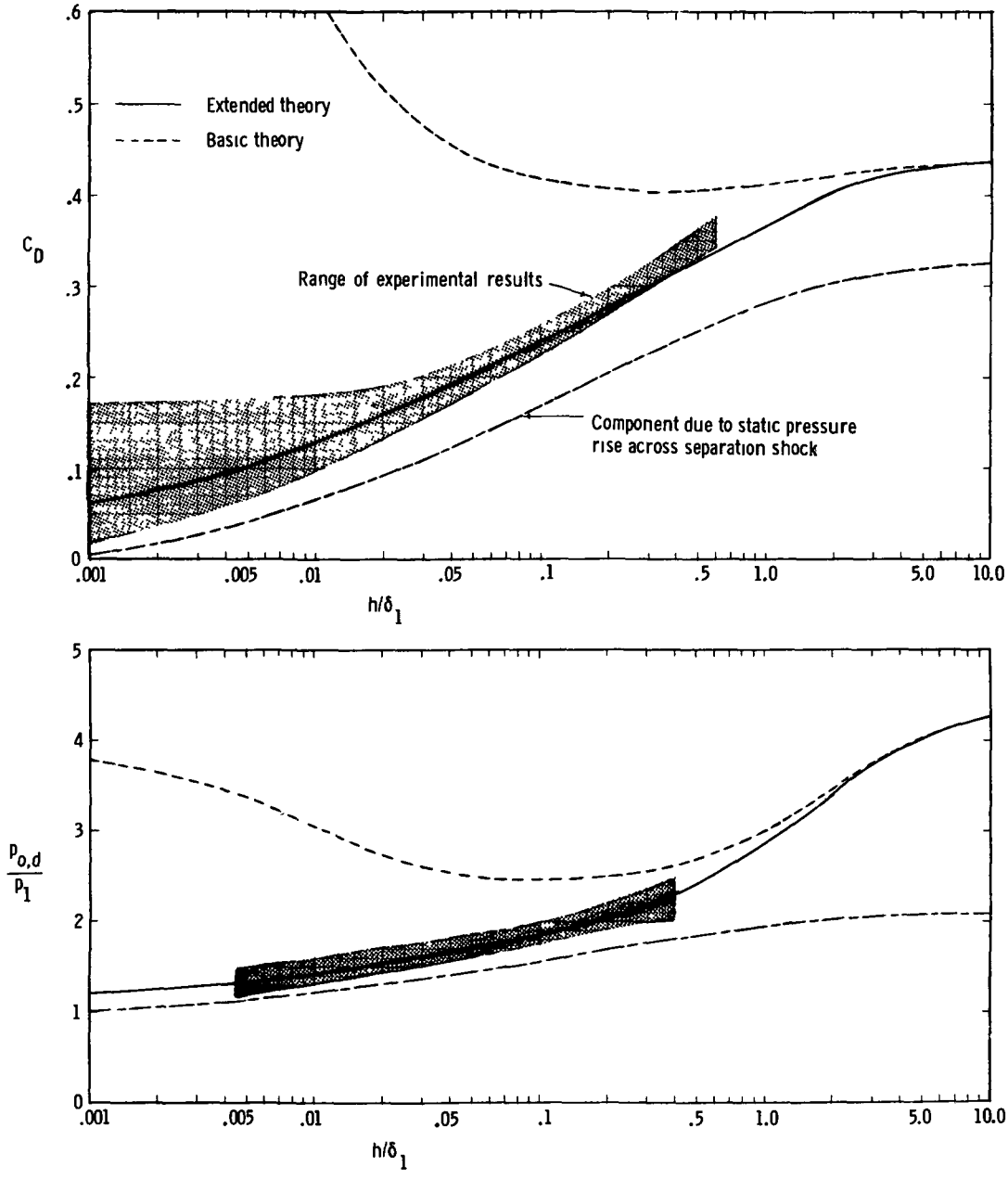

(b) $M_{1,e} = 2.2$.

Figure 15.- Concluded.

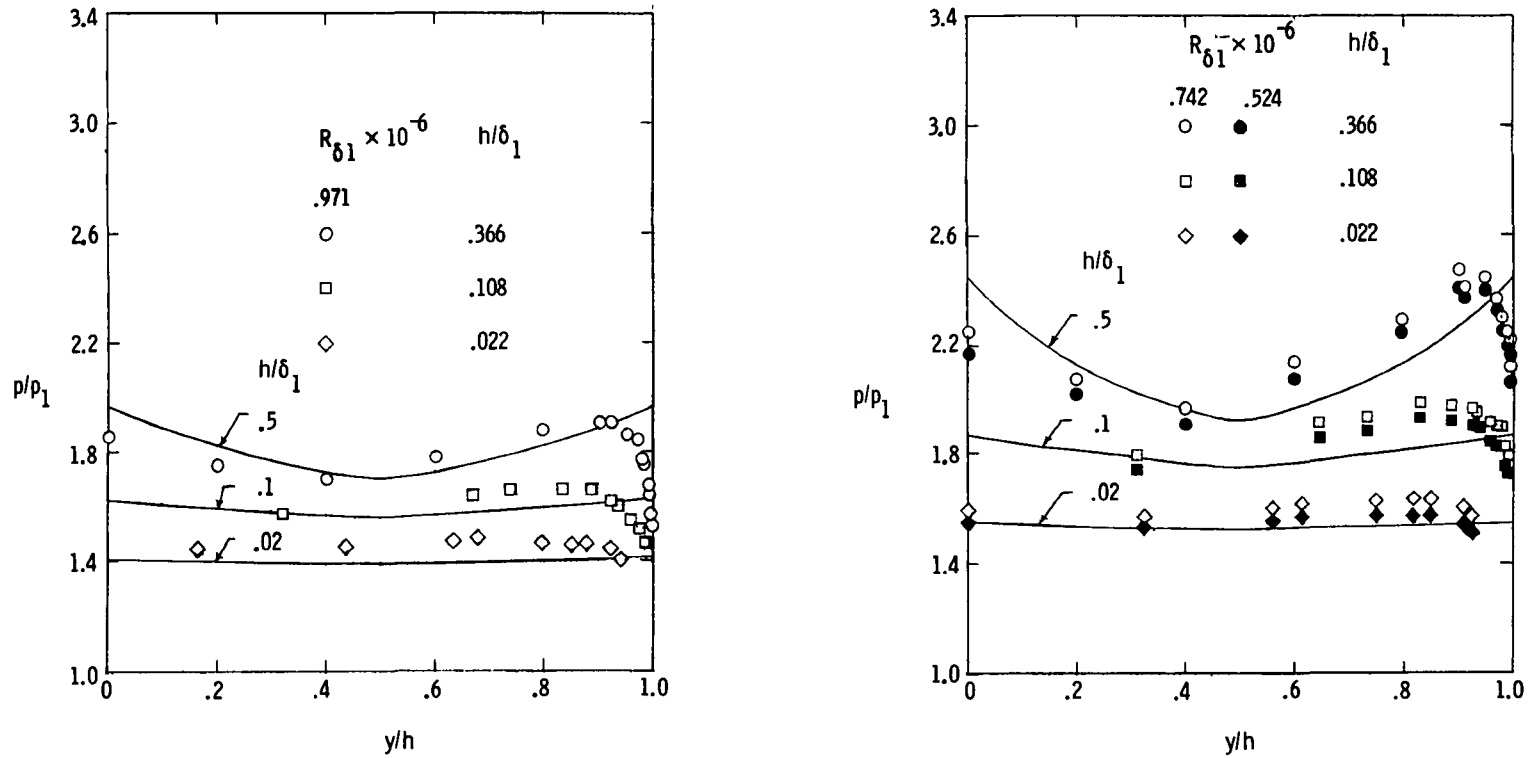

(a) $M_{1,e} = 1.61$.

(b) $M_{1,e} = 2.20$.

Figure 16.- Comparison of extended theory pressure distribution with experiment. Variable η_{rb}.

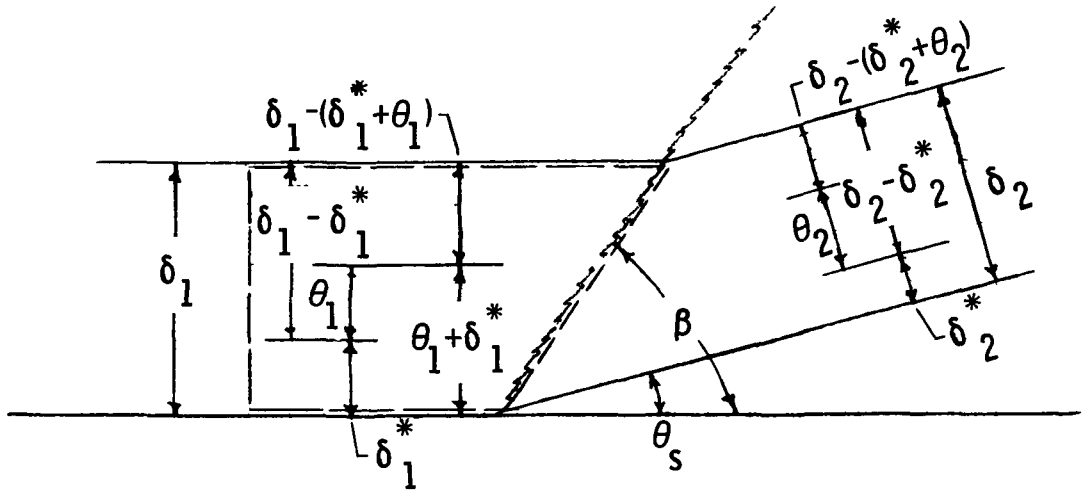

Figure 17.- Boundary-layer thicknesses along oblique separation shock.

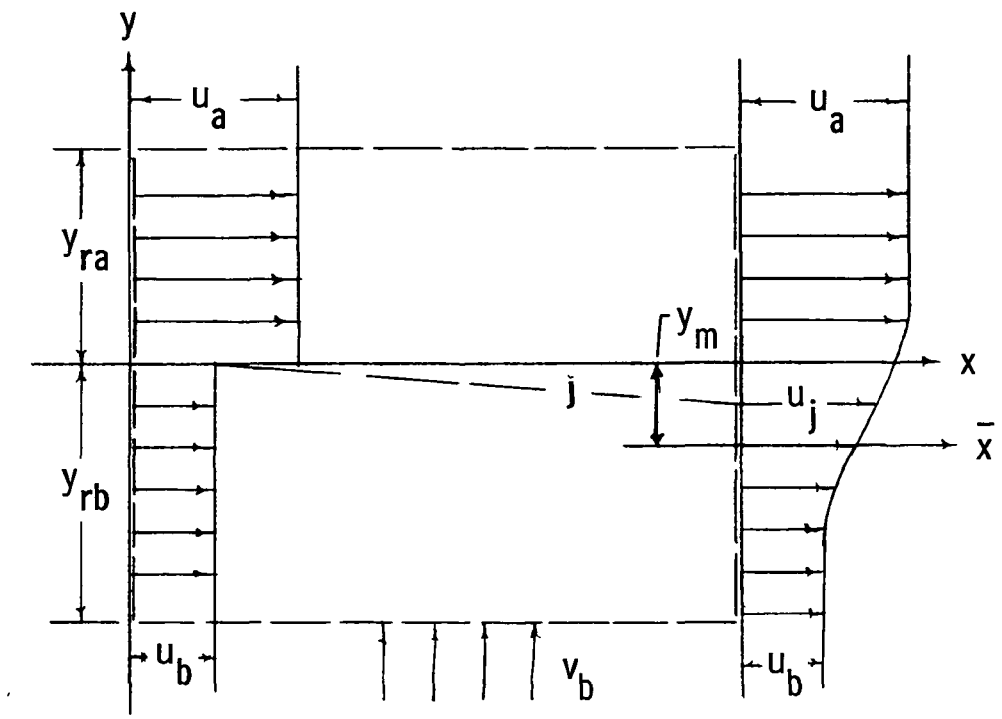

Figure 18.- Simplified model of two uniform streams mixing.

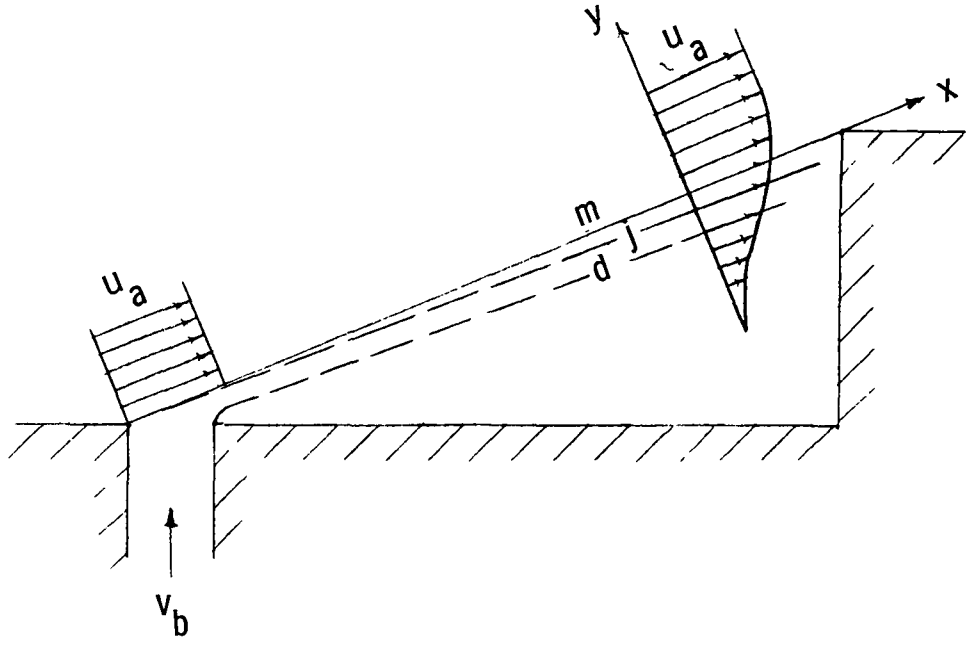

Figure 19.- Simplified model of air injection for thickening of the shear layer.

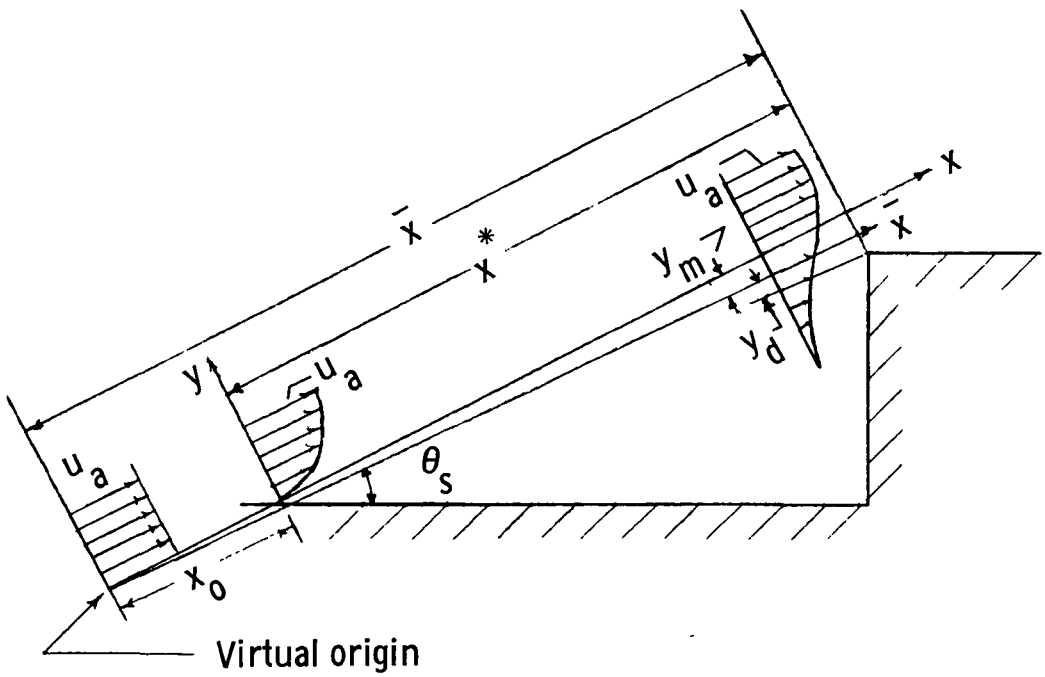

Figure 20.- Virtual origin and new shear layer.

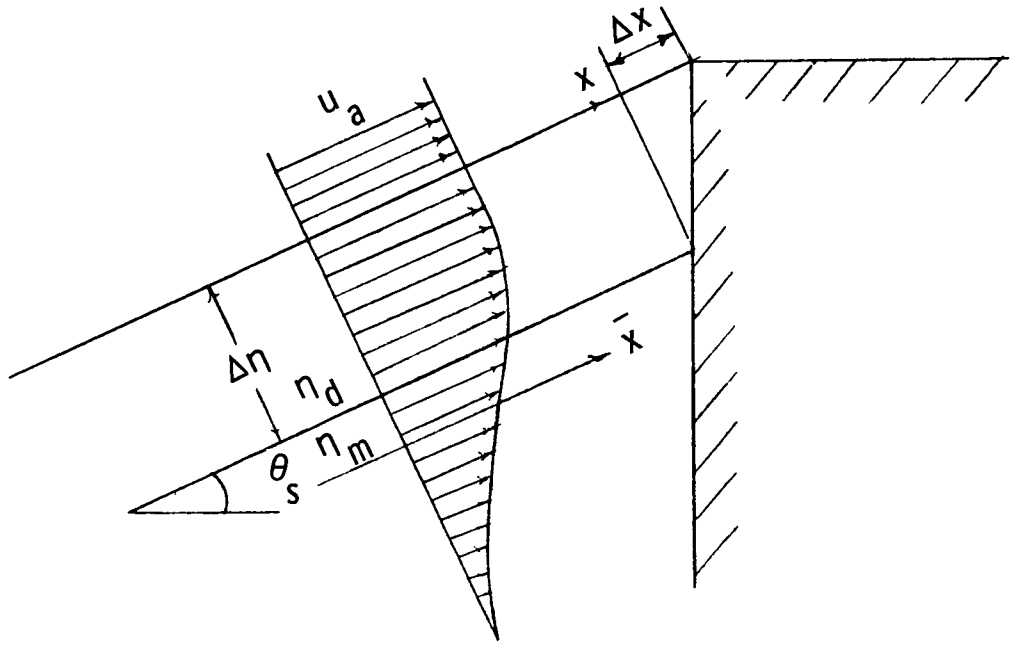

Figure 21.- Location of reattachment point.

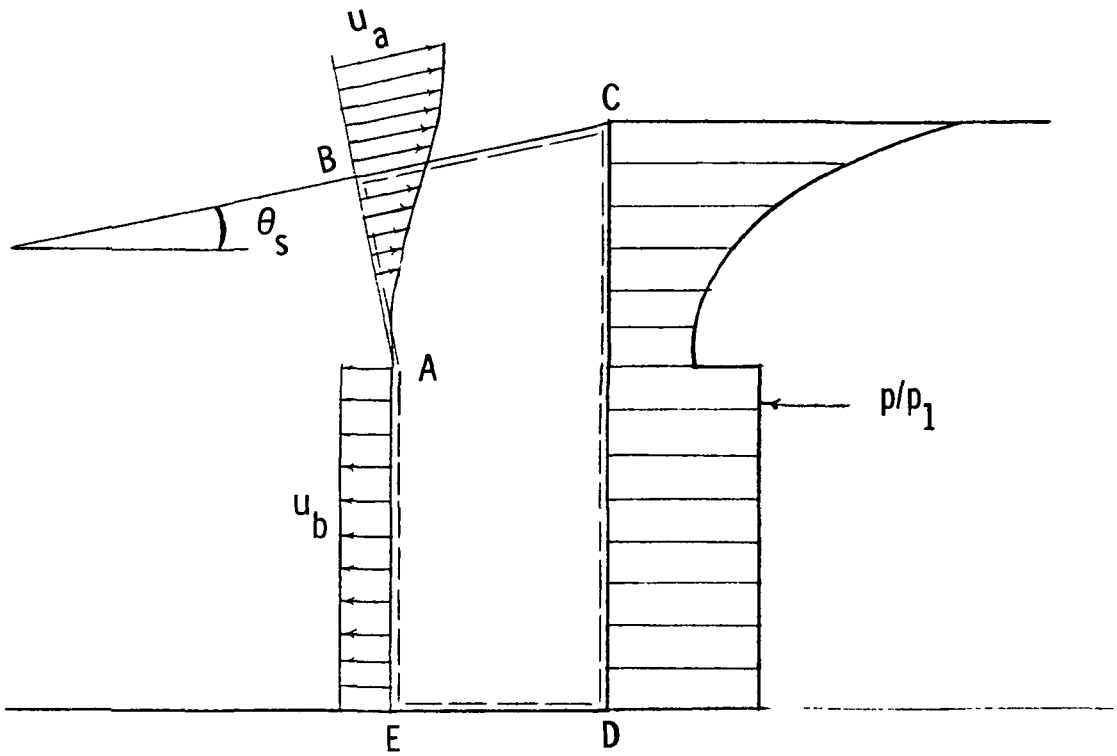

Figure 22.- Flow model for reverse-flow region.

1 Report No NASA TN D-8040	2 Government Accession No	3 Recipient's Catalog No
4 Title and Subtitle THEORETICAL FACE PRESSURE AND DRAG CHARACTERISTICS OF FORWARD-FACING STEPS IN SUPERSONIC TURBULENT BOUNDARY LAYERS		5 Report Date December 1975 6 Performing Organization Code
7 Author(s) D. K Patel and K R Czarnecki		8 Performing Organization Report No L-10331
9 Performing Organization Name and Address NASA Langley Research Center Hampton, Va 23665		10 Work Unit No 505-11-15-04 11 Contract or Grant No
12 Sponsoring Agency Name and Address National Aeronautics and Space Administration Washington, D.C 20546		13 Type of Report and Period Covered Technical Note 14 Sponsoring Agency Code

15 Supplementary Notes

D K Patel is an NRC-NASA Resident Research Associate

16 Abstract

A theoretical investigation of the pressure distributions and drag characteristics has been made for forward-facing steps in turbulent flow at supersonic speeds An approximate solution technique proposed by Uebelhack has been modified and extended to obtain a more consistent numerical procedure A comparison of theoretical calculations with experimental data generally indicated good agreement over the experimentally available range of ratios of step height to boundary-layer thickness from 7 to 0 05.

17 Key Words (Suggested by Author(s)) Forward-facing steps Turbulent flow Supersonic flow Shear flow Boundary-layer separation	18 Distribution Statement Unclassified – Unlimited Subject Category 34		
19 Security Classif (of this report) Unclassified	20 Security Classif (of this page) Unclassified	21 No of Pages 61	22 Price* $4.25

*For sale by the National Technical Information Service, Springfield, Virginia 22161

"The aeronautical and space activities of the United States shall be conducted so as to contribute . . to the expansion of human knowledge of phenomena in the atmosphere and space The Administration shall provide for the widest practicable and appropriate dissemination of information concerning its activities and the results thereof"

—NATIONAL AERONAUTICS AND SPACE ACT OF 1958

NASA SCIENTIFIC AND TECHNICAL PUBLICATIONS

TECHNICAL REPORTS Scientific and technical information considered important, complete, and a lasting contribution to existing knowledge

TECHNICAL NOTES Information less broad in scope but nevertheless of importance as a contribution to existing knowledge

TECHNICAL MEMORANDUMS Information receiving limited distribution because of preliminary data, security classification, or other reasons Also includes conference proceedings with either limited or unlimited distribution.

CONTRACTOR REPORTS Scientific and technical information generated under a NASA contract or grant and considered an important contribution to existing knowledge.

TECHNICAL TRANSLATIONS Information published in a foreign language considered to merit NASA distribution in English

SPECIAL PUBLICATIONS Information derived from or of value to NASA activities. Publications include final reports of major projects, monographs, data compilations, handbooks, sourcebooks, and special bibliographies

TECHNOLOGY UTILIZATION PUBLICATIONS Information on technology used by NASA that may be of particular interest in commercial and other non-aerospace applications Publications include Tech Briefs, Technology Utilization Reports and Technology Surveys.

Details on the availability of these publications may be obtained from:

SCIENTIFIC AND TECHNICAL INFORMATION OFFICE

NATIONAL AERONAUTICS AND SPACE ADMINISTRATION

Washington, D.C. 20546